Rita Valério Pontes

Licenciatura em Ciências de Engenharia de Materiais

Cellulose Nanorods in Liquid Crystalline Elastomers for Improved Actuators

Dissertação para obtenção do Grau de Mestre em
Engenharia de Micro e Nanotecnologias

Orientador: Professora Doutora Maria Helena Godinho, Professora Auxiliar com Agregação, Faculdade de Ciências e Tecnologia da Universidade Nova de Lisboa

Co-orientador: Doutora Susete Fernandes, Investigadora em Pós-Doutoramento, CENIMAT/I3N – Departamento de Ciências dos Materiais, Faculdade de Ciências e Tecnologia da Universidade Nova de Lisboa

Júri:

Presidente:	Prof. Doutor Rodrigo Ferrão de Paiva Martins
Arguente:	Prof. Doutor João Luís Maia Figueirinhas
Vogal:	Prof. Doutora Maria Helena Figueiredo Godinho

FACULDADE DE CIÊNCIAS E TECNOLOGIA
UNIVERSIDADE NOVA DE LISBOA

Setembro, 2014

‘The beautiful thing about learning
Is that no one can take it away from you’

BB King

Cellulose Nanorods in Liquid Crystalline Elastomers for Improved Actuators

Ackownledgments/Agradecimentos

'No man is an island,
Entire of itself (…)'

John Donne

Antes de mais, agradeço à minha orientadora, Doutora Maria Helena Godinho todo o apoio dado no decorrer deste trabalho e por me ter confiado esta tarefa. Agradeço também à minha co-orientadora, Doutora Susete Fernandes, não só por toda a ajuda na parte experimental, mas também pelas correções na componente escrita. Acima de tudo, um grande obrigada por me ter ajudado a ultrapassar todos os obstáculos, pela sua paciência e compreensão. Ao Doutor Rodrigo Martins, pelos desafios, oportunidades e incentivos à investigação, ao longo destes cinco anos.

À Teresa, nada disto teria sido possível sem o teu apoio. Obrigada por nunca me deixares desistir e por acreditares sempre em mim (e teres sempre pastilhas elásticas para todos…). Por me entenderes melhor do que eu própria me entendo. Por toda a paciência que sempre tiveste para mim e por me mostrares que o mundo não é um lugar assim tão feio. Esta tese também é tua.

Ao Alex (migsy!!), agradeço a companhia de tantas horas nesta faculdade. Almoços, jantares, imperiais e caracóis, sábados, domingos e feriados. Por todos as Empreendo-cenas, aventuras nas Américas e mil projetos de loucura, por todos os 'pitchos' escritos, vitórias e danças de xugo nas pseudo-derrotas. Quando formos milionários, vamos a um bar de charutos aleatório em Rayleigh, NC. Obrigada por tudo, Panda-Empreendedor. És uma pessoa incrível.

À Joana, por todos os momentos de loucura e longas conversas. Mostraste-me que eu também "preciso de um siso" e que na verdade estamos todos destinados a fazer candeeiros e *mojitos*. Em Barcelona. "Ermehgerd, cerlelers!"

Ao Marreiros, agora careca, pelo companheirismo ao longo destes 5 anos. Estás mesmo a tornar-te um adulto...

À Rute, por me ensinar que o silêncio é, por vezes, uma virtude.

Anselmo (não o Ralph), obrigada por me mostrares que ser *awkward* é um dom. És o maior da aldeia e mereces toda a sorte do mundo.

Ao Trofas, obrigada por todos os nossos cafés tardios. Tenho muito para te agradecer e um par de linhas numa tese nunca será suficiente.

Zé Rui, és realmente "o" Mágico. A tua boa disposição e optimismo são contagiantes e sei que vais chegar bem longe oh "farturas"!

À Susana das Frizes Groselha, unhas coloridas e mau feitio, obrigada pela paciência que sempre tiveste para me ouvir nas alturas mais complicadas. Agora prepara-te, que tens uma Odisseia pela frente.

À Meixeiro pelos *náites* e pelos *chill-outs*.

Ao Chico, que agora é "béta-testa", e à Legolas quero agradecer pelas bifanas, pelos chás das cinco e pelos *after-hours* no laboratório, sempre com boa-disposição.

Queria também deixar aqui uma dedicatória muito especial à máquina de café do edifício II, que raramente me desiludiu e muito me ajudou ao longo deste percurso.

Aúpe à Coro Echeverria, pelos ensaios de reologia e por me ensinar que a vida não é só feita de trabalho. *Muchas* gracias por todos os gins tónicos e pelos *pitis* partilhados, por todas as discussões e ensinamentos. Será sempre um prazer poder trabalhar contigo. "E bailar contigo. Una noche loooca ooh-ooh-oh-ooooh".

À Paula Soares, pelo FTIR, pelas palavras de incentivo e conselhos sábios. A idade torna-nos mesmo mais sábios… O fim deste ciclo merece certamente um festejo no *Sítio da Gente Jovem*.

Ao Luís Aguirre agradeço acima de tudo a amizade e apoio que sempre me deu. E obrigada também por me ensinares que as empanadas ficam com bolhas quando são fritas. Prevejo grande utilidade para isto no meu futuro. Quando for pastar ovelhas na Colômbia. Ou Paraguai. Ou Argentina.

Ao Filipe Silvestre, expresso aqui toda a minha admiração pelo seu trabalho e agradeço a infinita paciência e ajuda em todo o processo de desenho e impressão 3D. Às vezes pareces ter super-poderes!

A todo o grupo de *Soft and Biofunctional Materials* do DCM, em particular ao Doutor João Canejo e ao Doutor Pedro Almeida, pela ajuda no desenvolvimento dos protótipos.

À minha "família" da PE (Delgado, Mé, Laurinha, Paciências, Carla, Marques, Ramalho, Sónia e Varzielas): obrigada por todos os jantares e longos serões. Acima de tudo, obrigada por me aturarem já há tanto tempo.

E como o mais importante vem no final, quero deixar aqui o meu mais profundo agradecimento aos meus pais. Por tolerarem as minhas ausências prolongadas e mau feitio. Por me terem apoiado em todas as etapas deste percurso. Por sempre terem acreditado em mim e terem feito de mim a pessoa que sou hoje.

Sem vocês eu não seria nada.

Abstract

Nanotechnology plays a central role in 'tailoring' materials' properties and thus improving its performances for a wide range of applications. Coupling nature nano-objects with nanotechnology results in materials with enhanced functionalities.

The main objective of this master thesis was the synthesis of nanocrystalline cellulose (NCCs) and its further incorporation in a cellulosic matrix, in order to produce a stimuli-responsive material to moisture. The induced behaviour (bending/unbending) of the samples was deeply investigated, in order to determine relationships between structure/properties.

Using microcrystalline cellulose as a starting material, acid hydrolysis was performed and the NCC was obtained. Anisotropic aqueous solutions of HPC and NCC were prepared and films with thicknesses ranging from 22μm to 61μm were achieved, by using a shear casting technique. Microscopic and spectroscopic techniques as well as mechanical and rheological essays were used to characterize the transparent and flexible films produced. Upon the application of a stimulus (moisture), the bending/unbending response times were measured.

The use of NCC allowed obtaining films with response times in the order of 6 seconds for the bending and 5 seconds for the unbending, improving the results previously reported. These promising results open new horizons for building up improved soft steam engines.

Keywords: Cellulose, Polymers, Nanocellulose, all-cellulose composites, Liquid-crystalline elastomers, *stimuli*-responsive materials, moisture

Resumo

A nanotecnologia representa um papel central na manipulação das propriedades dos materiais e nas suas melhorias ao nível do desempenho, para um vasto conjunto de aplicações. Conjugar nano-objetos da Natureza com a nanotecnologia permite-nos obter materiais com funcionalidades melhoradas.

O principal objetivo desta tese era a síntese de celulose nanocristalina (NCC) e a sua incorporação numa matriz celulósica, de forma a produzir um material capaz de responder a um estímulo - humidade. O comportamento induzido nas amostras (*bending*/*unbending*) foi investigado a fundo, para determinar as relações entre estrutura e propriedades

Partindo de celulose microcristalina, foi possível obter NCC por hidrólise ácida. Prepararam-se soluções anisotrópicas de hidroxipropilcelulose (HPC) e NCC e, recorrendo à técnica de espalhamento *shear casting*, foram produzidos filmes com espessuras entre 22µm e 61µm.

Para caracterizar os filmes flexíveis e transparentes obtidos, foram utilizadas técnicas microscópicas e espetroscópicas, bem como ensaios mecânicos e reológicos. Sob a aplicação de humidade, os tempos de resposta (*bending*/*unbending*) das amostras foram medidos.

A utilização de NCC permitiu obter filmes com tempos de resposta na ordem dos 6 segundos para o *bending* e 5 segundos para o *unbending*, evidenciando melhorias relativamente aos resultados anteriormente publicados.

Estes resultados promissores abrem um novo horizonte no que diz respeito à criação de mecanismos melhorados (*soft steam engines*).

Palavras-chave: Celulose, Polímeros, Nanocelulose, Compósitos celulósicos, Elastómeros líquidos cristalinos, *stimuli-responsive materials*, humidade

Table of Contents

List of figures

List of tables

Symbology

R	Attached Hydrogen or a hydrocarbon side chain of any length
$\overline{DS}$	Average Degree of Substitution
$\overline{MS}$	Average Molecular Substitution
n	Director (unitary vector)
h	Distance between knife and substrate
P	Cholesteric Pitch
w/w	Mass Fraction
$\overline{\mathrm{M}}_{\mathrm{n}}$	Number Average Molecular Weight
S	Order Parameter
$\dot{\gamma}$	Shear rate
ε	Strain Deformation
σ	Stress
T	Temperature
t	Time
$T_{N\text{-}I}$	Transition Temperature Nematic-isotropic
v	Velocity
η	Viscosity
E	Young's Modulus
$\overline{\mathrm{M}}_{\mathrm{w}}$	Weight Average Molecular Weight

Abbreviations

AFM	Atomic Force Microscopy
AGU	Anydroglucose Unit
C*	Cholesteric
CCW	Counter Clockwise Direction
CW	Clockwise Direction
DS	Degree of Substitution
FIB	Focused Ion Beam
HPC	Hydroxypropyl Cellulose
LC	Liquid Crystal or Liquid Crystalline
LCE	Liquid Crystal Elastomer
MS	Molecular Substitution
N	Nematic Phase
NCC	Nanocrystalline Cellulose
Par.	Parallel to shear (direction)
Per.	Perpendicular to shear (direction)
PLA	Poly(lactic acid)
POM	Polarized Optical Microscopy
RPM	Revolutions per minute
SEM	Scanning Electron Microscopy
UTS	Ultimate Tensile Strength
XRD	X-Ray Diffraction

Objectives

The main objective of this work was to prepare and characterize the mechanical response of films prepared from liquid crystalline (LC) cellulosic systems, in order to build up cellulose-based *stimuli*-responsive devices. LC cellulosic materials can be shaped differently and therefore have potential applications in not only in macro but also micro and nanoengineering.

Anisotropic films were prepared by using a shear casting technique and were found to be moisture-sensitive. By playing with the orientational order, which is coupled with the mechanical strain, bending and unbending movements were induced in the films.

Taking profit of these motions, a soft motor device was idealized. In order to pursuit this objective, a prototype was designed and 3D-printed.

A major attempt was made to optimize the moisture-induced response of the films. Cellulose nanorods, as well as different processing conditions, were carefully investigated.

1. Introduction

1.1. Brief introduction to Liquid Crystals

"Crystals that flow".

This was the exact expression Otto Lehmann used in 1904 to describe liquid crystals (LCs), in his book *Flüssige Kristalle*, which was the first book dedicated to this state of matter. Despite the date of publication, Lehmann's studies in this field started around 1889, having introduced the use of the polarizing optical microscope (POM) coupled with a heating stage to study LCs, as well as identifying birefringence (crystals) and flow (liquids) in this type of materials.

Over several years, many physicists and chemists tried to understand this state of matter, as well as its properties. Nowadays, Liquid Crystals are used in several applications such as electro-optical devices and flat panel displays. These materials stand out for having remarkable properties, such as intermediate behaviour between crystalline solids and flowing liquids. It is long known that in the crystalline phase molecules present well defined spatial positions. In this type of materials, there is a long range periodic order in three dimensions. On the other hand, on the isotropic phase (liquids), there is no long-range orientational order. [1] So, as a mesophase (*meso*-intermediate from latin), liquid crystals exhibit a state of order between the crystalline and the isotropic, as shown on Figure 1.(a)

Regarding the formation of the mesophase, liquid crystals may be classified as thermotropic or lyotropic. In thermotropic LCs, the transition between phases (solid – LC – liquid) is induced by temperature, while in lyotropic LCs, the formation of the mesophase is induced by a variation of the concentration (dissolution/solvation).[2]

Molecules that can originate liquid crystalline phases are called mesogens and can present different molecular order. The most common are calamitic (rod-like), discotic, bent core (banana shaped) as shown on Figure 1.1(b) and LC-polymers (which include a class of aromatic polyester polymers).

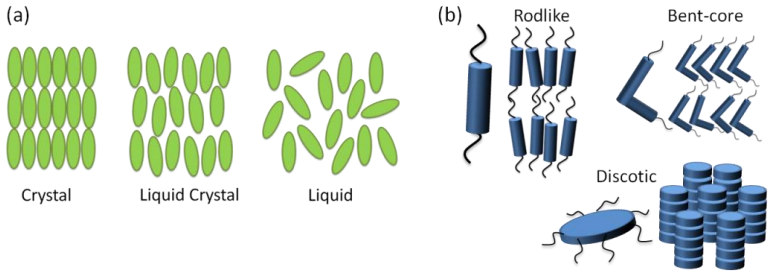

Figure 1.1- (a) Schematic of molecular order of crystalline, liquid crystalline and isotropic phases (b) Different molecular shapes, that can originate liquid crystalline phases

According to the mesophase's structure, a liquid crystal may be further classified as nematic, smectic, columnar or cholesteric (also known as chiral nematic). This work will focus mainly on the nematic and cholesteric structures, whose properties will be described in more detail further ahead.

Another important feature of liquid crystals is the remarkable optical properties. While in isotropic media (like fluids) there is only one refraction index, in anisotropic media (like LC), different refraction indexes depending on the direction of the light propagation, can be observed. This phenomenon is designated as birefringence and is the reason why liquid crystals are being used, nowadays, in optical fibers [3] and other photonic devices. [4]

.It is possible define the director **n** as a two-headed vector that provides the average direction of the alignment of molecules. Thus, one may also define θ as the angle between a single molecule and the director **n**.

The molecules do not necessarily all point in the same direction, however there is a preferred molecular orientation, at a given point r, described by a unit vector **n(r)**, which may suffer thermal fluctuations. A thermodynamic parameter can be defined to characterize the order of the nematic and is given by:

$$\langle S \rangle = \langle \frac{3}{2}\cos^2\theta - \frac{1}{2} \rangle \tag{1.1}$$

where the brackets denote an average over many molecules at the same time or the average over time for a single molecule. [5] In an ordered state, all the molecules are oriented and θ=0° which, trivially, leads to S=1. Alternatively, in a disordered state (as an isotropic fluid) the molecular axis point in all directions with equal probability, which leads to S=0.

The nematic phase is the simplest case of a mesophase, where the molecules exhibit long range ordering but no positional ordering. Recalling the concept of director **n**, the rod-like molecules in this mesophase tend to align with their long axis somehow parallel to the director, as shown on Figure 1.2 (a).[6]

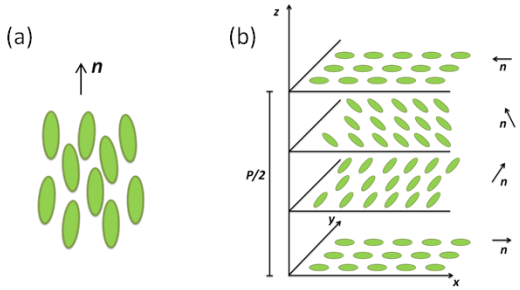

Figure 1.2- Schematic representation of a: (a) Nematic phase; (b) Cholesteric structure, where P/2 is half of the cholesteric pitch

For a nematic phase to occur, each molecule must be achiral (each molecule must be identical to its mirror reflection) or, otherwise, it is only possible to have a nematic phase when the system is a racemic mixture (1:1) of left-handed and right-handed species.[7]

Solving a chiral molecule in a nematic, the structure will suffer a distortion, resulting in a helical structure. Thus, a special layered structure is formed – cholesteric - where, in each plane, the molecules are oriented as in a nematic. Perpendicularly to the layers, there is the z-axis, also designated as optical axis, around which the orientation of **n** varies from layer to layer, rotating around

the optical axis and following a helical trajectory, as represented on Figure 1.2(b). The pitch (P) is defined as the spacing between layers until the director performs a rotation of 360°.

The P values are usually in the order of magnitude of the optical wavelength, leading to an interaction between the light and the structure. This spacing may be modified by changing the temperature and concentration. Thus, it is possible to engineer the gap in order to observe different colours by changing the Bragg scattering of light. However, by changing temperature some cholesteric phases present a critical temperature (T*) at which the pitch tends to infinite and the chiral nematic phase behaves as a conventional nematic. Despite the similarities/intimate relation with nematic phases, chiral nematics only occur in non-racemic systems (i.e., molecules different from their mirror image).[7]

1.2. Liquid Crystalline Elastomers

Based on liquid crystals and adding properties of polymers and rubber elasticity, a new category of materials was created: Liquid Crystal Elastomers. This exclusive class of functional materials exhibits a remarkable behaviour not seen in either elastomers or LCs separately. Nowadays, this type of materials is used as actuators, cantilevers or micro-motors.

Elastomers are rubber-like solids characterized by an elastic modulus of the order of MPa which can accommodate strains of over 100%. We may define Liquid Crystal Elastomers (LCEs) as cross-linked polymer networks with orientationally ordered mesogenic units, with the unique ability to couple mechanical strain and orientational order. As a consequence, any change in orientational order will result in mechanical strain, causing a change in the sample's shape. Changes in the order parameter may be caused by heating, illumination, exposure to electric fields or the presence of chemical solvents, giving rise to corresponding changes in sample shape. [8] Also, the incorporation of nanoparticles into LCEs has been of considerable recent interest, with the aim of achieving a faster response speed and better control over the actuation.[9]

1.3. Cellulose and Cellulose derivatives as functional materials

Cellulose is the polymer selected by Nature to build up the plant's world, is an abundant and renewable resource found in most parts of the world, which makes it a cheap raw material for various applications [10]. Cellulose belongs to a family that can form cholesteric liquid crystalline (LC) phases, exhibiting remarkable optical properties as a result of their photonic band structure, and applications such as polarized light sources, information displays and storage devices

Considering all these properties and knowledge and taking advantage of the spontaneous formation of liquid crystalline phases, in the framework of this thesis new functional materials will be investigated in order to produce mechanical responsive cellulosic devices.

1.3.1. Hydroxypropyl cellulose (HPC)

Hydroxypropyl cellulose (HPC) is a cellulosic derivative obtained by hydroxypropylation of the hydroxyl groups in the repeating unit of cellulose, as shown in Figure 1.3. As other cellulose derivatives, HPC also takes part in a large and established industry and is used in pharmaceuticals, food, personal care, construction, oil field chemicals, textiles, adhesives, ink paper, coating, among several others.

This compound was reported to form both thermotropic and lyotropic mesophases, in suitable solvents. In aqueous solution, HPC is known to form a lyotropic phase. The critical concentration, at room temperature, varies with polymer characteristics. However, HPC is usually able to form a LC phase at concentrations between 41% (w/w) and 80% (w/w).[11] The use of this cellulose derivative in stimuli-responsive systems has been already described in literature [8][12][13][14].

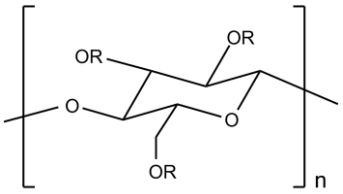

Figure 1.3 - Chemical structure of Hydroxypropyl cellulose, where R=H or R=$CH_2CH(OH)CH_3$. The maximum value of the degree of substitution (DS) of HPC is 3, while there is no theoretical maximum limit of molecular substitution (MS).

1.4. Nanomaterials

One of the main interests of nanotechnology is the possibility to alter material's properties, making them totally customizable. This opens a whole new world of possibilities and over the last decades, there has been a crescent interest in creating materials with improved performance, to potentiate new applications and optimize existing ones. This type of approach implies the manipulation of atomic bonds – at the nanoscale – assigning nanotechnology with the central role in this process.

1.4.1. Nanocrystalline Cellulose (NCC)

Lately, nanocrystalline cellulose (NCC) has drawn a lot of attention due to the properties of the materials it can originate (light weight, stiffness, transparency)[15][16][17], being used in a wide range of areas, from pharmaceuticals [18] to electronics [19].At the nanoscale, interfaces represent an essential role and due to the high surface area, nanomaterials are being used as fillers in composites, assuring perfect interfaces with the matrices. This way, it is possible to distribute mechanical solicitations through all the material. [20]

When using a filler with a chemical structure similar to the matrix, this interface is expected to be almost perfect. In this way, nanocrystalline cellulose states itself as an obvious filler for composites based on cellulose derivatives, creating the 'all-cellulose composites'.[21]

NCCs may be easily obtained via chemical reaction, by separating crystalline and amorphous regions of the cellulose's structure, as shown schematically on Figure 1.4. Thus, acid hydrolysis allows isolating cellulose nanocrystals.

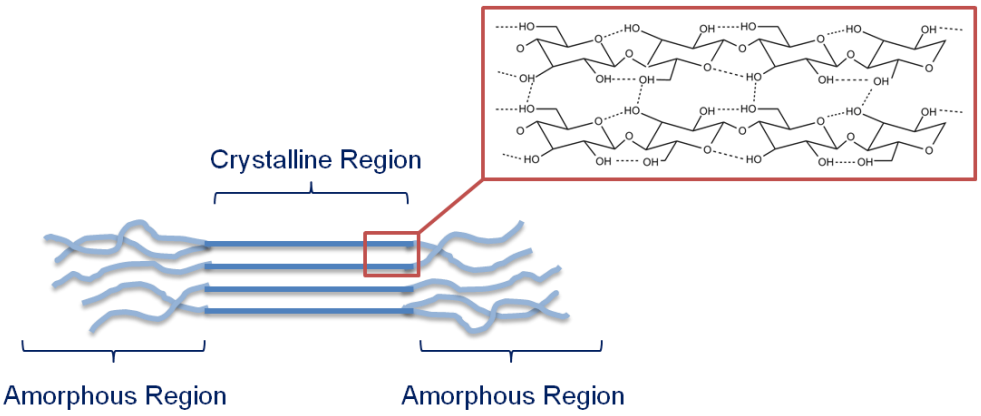

Figure 1.4 – Schematics of molecular ordering in crystalline and amorphous regions, inside cellulose microfibrils.

1.4.2. *Tailoring* properties at the nanoscale

Cellulose nanocrystals may be incorporated in other polymeric matrices, in order to enhance mechanical properties. In the present case, by using a cellulosic matrix (HPC) we are able to achieve an all-cellulose composite. Both materials have a similar chemical structure, which provides better interaction between the two materials. Therefore, the composite is expected to present improved mechanical properties regarding Young's modulus and tensile strength.[13]

By using a solvent-vapour as a *stimulus*, it was found that anisotropic HPC matrices can change shape, by playing with the order parameter [8]. One can expect that despite of the NCC not being "activated" by the stimulus, the material still responds, depending on the NCC's concentration. When the stimulus is removed, the HPC domains will relax to the original state, being driven by the nanorods' orientation, which is translated to a much faster relaxation time. Besides the possible advantages referred, we must keep in mind that by adding a filler to the nanocomposite, we anticipate a trade-off between mechanical properties and the performance as an actuator.

1.5. Soft Motors

In 2008, Yamada et al. [22] demonstrated, for the first time, a light-driven plastic motor. This device was able to directly convert light energy into mechanical work (photomechanical effect), taking advantage of the cooperative movement of mesogen's and polymer segments in a liquid-crystalline elastomer containing azobenzene derivatives. The cromophores incorporated in the structure of this LCE suffer a *trans-cis* photoisomerization when irradiated with UV light, leading to a photoinduced phase transition. The changes in the alignment of mesogen's at the microscopic scale are thus reflected in significant macroscopic changes in order.

Later on, Geng et al. [8] used a cellulose derivative to build a soft motor which was able to convert a humidity gradient into mechanical work. This cellulose-based engine exploits the difference in chemical potential of water molecules in humid and in dry air. By transporting water from regions of high chemical potential to low, the device was able to gain energy in the process.

2. Materials and Methods

2.1. Production of HPC and HPC/NCC films

HPC was purchased from Sigma–Aldrich ($\bar{M}_w$=100.000; $\overline{MS}$=3.5; $\eta_{5\%,25°C} = 125cps$) and Alfa Aesar ($\bar{M}_w$=100.000; $\overline{MS}$=3.5; $\eta_{5\%,25°C} = 89cps$) and used as received. Avicel (microcrystalline cellulose ~ 50µm particle size) was acquired from Sigma-Aldrich.

Nanocrystalline cellulose particles were prepared on the basis of the methods of Gray et al. [23][24] and Orts et al. [25] with minor adaptations. Microcrystalline cellulose was hydrolyzed with sulfuric acid (97%, p.a., Merck) with an acid/solid ratio of 16:1 at 45°C for 130 minutes under vigorous stirring. The resultant suspension was washed with ultrapure water by successive dilution and centrifugation (at 12000 rpm for 20 minutes) until the supernatant was turbid (which occurs at approximately pH 1.9–3.8). The resulting suspension was placed in a Spectra/Por 4 cellulose membrane (Spectrum) and dialyzed against ultrapure water until a pH of 6–7 was reached. A suspension of NCC in water was obtained. The content of NCC in the suspension was, when need, increased by subsequent centrifugations (at 14000 rpm for 20 minutes) and a gel-type substance was obtained. The water used in these experiments was purified by using a Millipore Elix Advantage 3 purification system. The synthesis of NCC, as described, took approximately one month to be completed. Suspensions of NCC in water with concentrations that ranged 0.3 to 3 % (w/w) were obtained and used without further treatment.

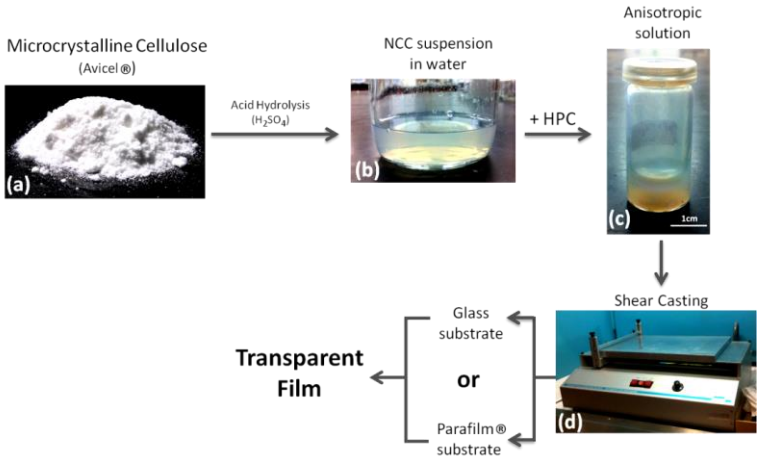

Figure 2.1 - Schematic representation of the different paths involved in the NCC synthesis and film preparation. Starting from (a) microcrystalline cellulose, an acid hydrolysis is performed, resulting in a (b) suspension of NCCs in water. By adding HPC, an (c) anisotropic solution is obtained and (d) shear-casted in the shape of a film.

Lyotropic liquid crystalline solutions of HPC in distilled water with concentrations of approximately 60% (w/w) were prepared at room temperature. Liquid crystalline solutions of the composite HPC/NCC in water were also prepared maintaining the total amount of solids in approximately 60%. Different composite systems were prepared by changing the percentages of NCC from 0.1 to 5%. After the first week the solutions were stirred every other day and kept in the dark for at least 4 weeks until further used.

Both HPC/H_2O and HPC/H_2O/NCCs solutions (with different concentrations of NCCs) were cast and sheared simultaneously by moving a calibrated Gardner knife from Braive Instruments at 1.21 mm s^{-1} over a glass substrate or, alternatively, a Parafilm® substrate. The films were allowed to dry at room temperature and kept in a controlled relative humidity (~30%) chamber until further use. In Figure 2.1 is presented a summarized scheme of the experimental procedure for the preparation of the nanocomposite films.

2.2. Shear Casting Knife adaptation: *reduce the minimum speed*

The shear-casting knife used to produce the films is schematically represented in Figure 2.2. This equipment has a moving arm, which casts a solution or gel over a solid substrate. After drying, the obtained thin polymeric thin films are ready to use. The velocity of the moving arm may be controlled, having its minimum at 1.25 mm s^{-1}.

Placing calibrated weights on the top of the ruler, it was possible to reduce the knife's minimum speed and, simultaneously, the thickness of the produced films. This adaptation of the technique was extremely useful for the purpose of the thickness study.

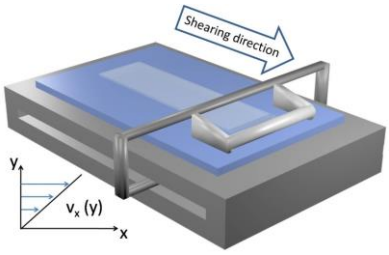

Figure 2.2- Schematic representation of the shear-casting apparatus used to produce films of lyotropic liquid crystalline solutions of HPC and HPC/NCC with different thickness. The thickness of the films can be controlled by the gap and velocity of the Gardner Knife.

According to the basic principle of the shearing deformation, described by Equation 2.1 [26], by decreasing the velocity (v), the shear rate ($\dot{\gamma}$) would also decrease. Simultaneously, the distance (h) between the knife and the substrate will decrease due to the applied pressure. Thus, the ratio between velocity and distance is expected to stay, approximately, constant. Accordingly, we may consider that the shear rate remains unaffected.

$$\dot{\gamma} = \frac{v}{h} \tag{2.1}$$

2.3. Production of a soft motor

Taking advantage of this *stimuli*-responsive material, Geng et al. [8] presented a soft motor of this stimuli-responsive material, HPC, powered by a humidity gradient. This device, schematized on Figure 2.3(a), consists of a circular loop of a cellulose-based film, which passes over two wheels, mounted on a stand. When the cellulosic film is mounted in the stand its configuration is symmetric about a vertical axis, as can be seen in figure 2.3(b1). The lever arms (in green) are of equal length, and the net

torque on the top wheel due to the tension in the film is zero. Applying moisture in the surroundings of the outer surface of the film near one of the wheels leads to a shortening of the lever arm in this area, due to the bending of the film.. Consequently, the wheels will rotate, as illustrated in Figure 2.3(b2). As the wheels keep rotating, the film will dry. Theoretically, this means that the device will rotate while the stimulus is applied.

Geng et al. had showed that this cellulose liquid crystal motor rotates, however the rotation was neither complete nor fast and further improve in the system, not only regarding the film matrix but also the parts of the device, should be done.

The use of wheels with different diameters, in theory, will result in a speed-multiplier effect, as in the mechanism of bicycles. Based on previous work [22] for a similar device, the optimum diameter's ratio used should be approximately 3.33. In this work, with the purpose of optimizing the performance of the device shown in figure 2.3(a), new wheels were produced with different diameters. For further details, see Supplementary Materials – Section 6.1.

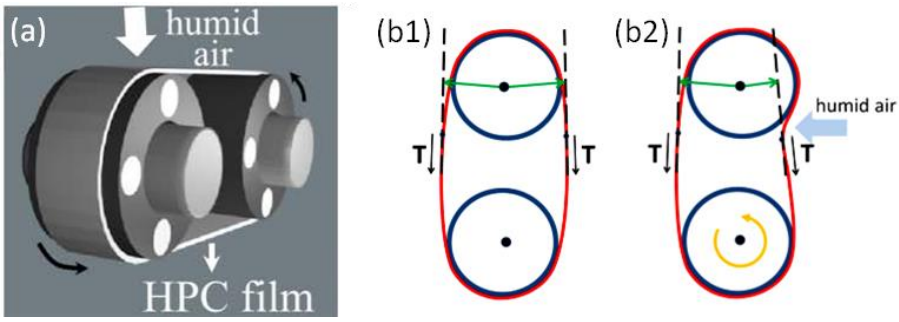

Figure 2.3 – (a) Schematic of the soft motor, showing the location of the cellulosic film, moist air and rotation direction. The alignment direction is parallel to the axes of the wheels. The free surface of the film is on the outer side of the device. Initially (b1), the lever arms (in green) have equal length. The application of a stimulus (b2) leads to a deformation of a cellulosic film, shortening one of the lever arms. The torque (T), which was initially zero, will now promote a counter clockwise rotation. [8]

Additionally and in order to promote an easy process of assembly of the device, a new stand was built, as shown in figure 2.4(c1). The components of this stand were built separately, so this device is detachable and customizable. Apart from the stand, each axis (Figure 2.4(c2)) is fixed on a glass slide, which may be attached to the stand, by using the lateral clamps (Figure 2.4(c4)) that will allow adjusting the distance between wheels. With this new stand it will be possible to assemble motors using a wide range of wheel's diameters, in order to determine the influence of the wheels' size and ration in the performance of the device.

2.3.1. 3D Printing

A 3D printer was used to produce both wheels and stand. 3.75mm and 12.50 mm were the diameters chosen for the smaller and larger wheel respectively. The height for both wheels is 5mm. The wheels were then printed in a PRUSA 3D Printer, Figure 2.4(a). The polymer used was Poly(lactic

acid) (Orange Innofil3D PLA 1.75mm) supplied by iGo3D.com. The fill density selected for the printing was 15%, in order to obtain lighter components. The final weight, Figure 2.4(c3), of this new set of wheels is approximately 0.31 grams, equivalent to 1/3 of the ones used previously by Geng et al.[8] (approximately 1 gram). Additional images of the developed three-dimensional model may be consulted in the Supplementary Materials section 6.1.

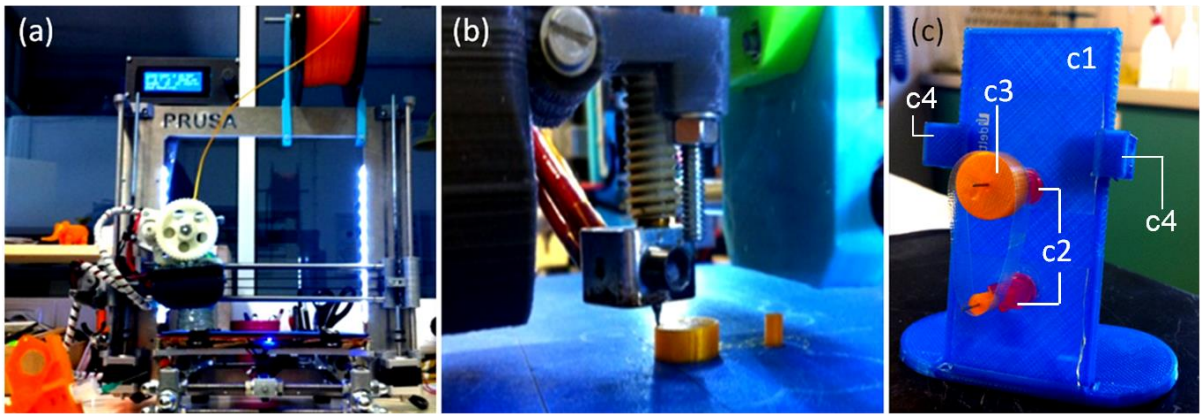

Figure 2.4 - (a) PRUSA 3D Printer, (b) printing process of the wheels, (c) final stand with all the components assembled. In blue (c1), the main structure of the stand with the mounted axis (c2), the printed wheels (c3) and the lateral clamps (c4).

2.4. Characterization

General Characterization

Photographs and movie of the cellulosic film and motor were taken with a Casio EX-F1 Exilim Pro and Canon EOS 550D photo camera.

Dimensional Characterization

Length distribution analysis of NCC was obtained following image acquisition using SEM. The lengths and diameter of individual filaments visible in these SEM images were measured with ImageJ software (version 1.45s, http://imagej.nih.gov/ij/) and scaled according to the magnification quoted by the microscope software. A minimum of 50 length and diameter measurements was taken. The thicknesses of the films produced were estimated from the average of 10 measurements made using a *Mitutoyo* digital micrometer.

Chemical Characterization

Chemical characterization of the prepared samples was conducted through Fourier Transform Infrared (FTIR) spectroscopy. FTIR spectra of shear-casted HPC films and HPC with different contents of NCC were collected using a attenuated total reflectance (ATR) sampling accessory (Smart iTR) equipped with a single-bounce diamond crystal on a Thermo Nicolet 6700 spectrometer. The spectra were acquired with an incident angle of 45 º, within the range of 4000-650 cm^{-1},resolution of 4 cm^{-1}, at temperature of 20°C and are the result of 32 scans.

Structural Characterization

For the structural analysis X-Ray Diffraction patterns were collected. This was done using a XRD PANalytical (model X'Pert Pro) in Bragg–Brentano geometry with Cu Kα line radiation (λ=1.5406 Å) at 45 kV and 40 mA, the instrument being equipped with an X'Celerator detector. The XRD patterns were collected with a scanning step of 0.0334° over the angular 2θ range 10°–40°, with a total acquisition time of 4 min. To analyse the diffractograms, specific software (OriginPro 9) was used that allows the characterization of the peak parameters such as position, intensity, width and shape.

To analyze the morphology and topography of the film samples, Atomic Force Microscopy (AFM) and Scanning Electron Microscopy (SEM) were carried out. Both of techniques allowed observing the surface of the samples, as well as the NCC's orientation.

For the topographical characterization of the films surface, AFM data were acquired using a dimension 3100 spm with a Nanoscope IIIa controller from Digital Instruments (DI). All measurements were performed in tapping mode TM under ambient conditions. A commercial tapping mode etched silicon probe from DI and a 90µm x90µm scanner was used.

Scanning electron microscopy images of the nanocrystalline cellulose films were acquired with a Carl Zeiss Auriga crossbeam (SEM-FIB) workstation instrument equipped with an Oxford energy dispersive X-ray spectrometer. The SEM images were taken in the in-lens mode with an acceleration voltage between 1.50kV and 5.00kV and aperture size of 30 µm. HPC and HPC/NCC films were coated with a thin carbon layer (approximately 30nm) and nanocrystalline cellulose was coated with a thin Au/Pd layer (8-10 nm) using a Q300T D Quorum sputter coater. The topological features of some samples of HPC films were also analyzed with a SEM DSM962 model from Zeiss. Gold was deposited on the films by sputtering in an Ar atmosphere, using a 20 mA current, for 30 s at a deposition rate of 3 Å s^{-1}. Images were captured for an acceleration voltage of 5 kV.

Using the Polarized Light Microscope BX51 from Olympus, equipped with a cold light KL2500 LCD from Olympus, it was possible to observe characteristic bands/groves in the films' surface. Images were acquired with a DP73 CCD Camera, Olympus, and Olympus Stream Basic 1.9 software.

Mechanical Characterization

To evaluate the mechanical properties of the film samples, a tensile testing machine from Rheometric Scientific (Minimat Firmware Version 3.1) was used. Small rectangular pieces of the cast films, with the dimensions of 2 cm × 1 cm, were cut in two distinct directions orthogonal to each other (i.e., one with the longest dimension of the sample parallel to the direction of the shear casting and another perpendicular to it). In addition, the film was stretched uniaxially at a rate of 5 mm min^{-1}, along the longest sample dimension. The values of the mechanical properties of a given sample were taken to be the average of the results of ten successful measurements. Samples were taken from different parts of the film.

Rheology

The rheological characterization of the HPC and HPC/NCC solutions was performed using a stress-controlled rheometer Bohlin Gemini HR nano, with a cone-plate (20mm diameter and 2º cone) geometry.

Flow curve experiments were carried out as follows: All the samples were measured at room temperature at a range of shear rates between 0.001 to 1000 s^{-1}. The integration time and equilibration time for each point was 4 seconds respectively.

3D Modelling

The software Blender, version 2.57b, was used to obtain the 3D draw of the shear-casting knife apparatus and the motor.

For the design of stand and wheels, Autodesk® AutoCAD® 2014 Software - Student Version (Serial Number: 900-46298126) was used.

Films' Bending/Unbending Response times

Samples of shear casted films were tested under the application of moisture. The water vapour was generated by an AirProject ultrasonic humidifier (Italy ARTSANA Group). Photographs and movie of the cellulosic film and motor were taken.

3. Results and Discussion

This dissertation focuses on the production of an all cellulose-based *stimuli*-responsive material. This material was obtained from a thin film resultant of the incorporation of nanocrystalline cellulose into a liquid crystalline polymer matrix of HPC. So, the work below describes the synthesis of nanocrystalline cellulose and its incorporation in the matrix of HPC. In order to obtain this, lyotropic liquid crystalline solutions of HPC and HPC/NCC with different NCC contents, in distilled water, were prepared. These aqueous solutions were shear-casted and anisotropic HPC or HPC/NCC free-standing films, with different thickness, were obtained. The influence of the presence of NCC in the liquid crystalline precursor solutions was investigated by means of rheology.

The new films obtained from the nanocomposite system were chemical, structural and morphologic characterized and a similar work was done for the neat HPC system and the synthesised NCC. The mechanical properties of the film samples were also determined.

The induced behaviour obtained when an external *stimulus* (moisture) was applied at the top surface of the cellulose-based samples – bending was investigated. Thus, upon the application of moisture, the film bends and while drying the film unbends and this response times were determined. A first attempt to understand the influence of the polymer matrix, content of NCC and film's thickness in its bending/unbending response was made.

One should notice that the method to prepare the samples of HPC or HPC/NCC films used in this work was based on an experimental procedure used within the workgroup. However, during the course of this thesis and in order to decrease the thickness of the films to a desire value, it was necessary to proceed to an adaptation of this method that is described in section 2.2.

Throughout the duration of this work, an attempt to optimize the soft motor device initially developed by Geng et al. [8] was made. New wheels and also a new wheels-stand (with separable components) were designed, developed and built with a 3D printer. The fact that this wheels-stand is detachable makes it customizable, which opens its future applications. Therefore this new wheels-stand will allow the use of cellulosic belts with different diameters and different wheels. Additionally a Teflon mould was prepared in order to produce circular belts from films of liquid crystalline cellulose-bases solutions without any union (for further information, see Supporting Information – section 6.4). Nevertheless, considering the duration of this work it was not possible to use these new pieces.

3.1. HPC Matrix

In this work the matrix used to prepare the all-composites cellulosic films was the HPC. This is a very well known cellulose derivative that can easily be dissolved in water and at a range of concentrations generates liquid-crystalline helicoidal phases. Depending on concentration these LC solutions can have the pitch in the visible range. In this work a concentration of 60% (w/w) of HPC was selected and as expected a iridescent colour, mainly red, can be observed in the anisotropic solution (figure 2.1(c) - experimental section). This result is in good agreement with the observed by Werbowyj

et al. [11]. This all-cellulosic nanocomposite system has the appropriate conditions to incorporate the hydrophilic nanocrystalline cellulose, mainly due to the same chemical nature of both NCC rods and matrix.

The first samples of HPC films prepared in this work were obtained from a HPC supplied by Sigma-Aldrich, similar to the HPC used in the work of Geng et al. However instead of homogeneous film unexpectedly the new films produce were very inhomogeneous, regardless the large experience of the group in this preparation technique. In order to try to understand this effect HPC from two different suppliers were used (Sigma-Aldrich and Alfa-Aesar).

Anisotropic HPC films were formed by spreading the liquid crystalline aqueous HPC solutions (60% w/w) with the help of a calibrated shear casting-knife moving at a controlled speed of 1.25 mm s^{-1}. In this preparation technique initially the solutions are on a glass substrate, with a free surface exposed to air. If the solution has a cellulose concentration sufficiently high for the formation of the liquid crystal phase, the mesogenic fragments can be uniformly aligned in the sample by shear and a nematic sample is obtained. The films, after removed from the substrate are transparent and flexible. Films were then studied and characterized in order to choose the best HPC batch for the subsequent production of *stimuli*-responsive nanocomposites.

3.1.1. HPC from two different suppliers

Macroscopically, it was possible to notice differences in the homogeneity of the films obtained by the two suppliers, as can be seen in the films' pictures Fig 9c and d. From the POM image of the films prepared from solutions of HPC from the supplier Sigma-Aldrich, Figure 3.1(a), it is possible to notice that some bubbles were formed and in the film's picture (Figure 3.1(c)) the macroscopic aggregates are evident. On the contrary, films prepared from solutions of HPC from the supplier Alfa-Aesar are much more uniform, as indicated by Figures 3.1(b) and 3.1(c).

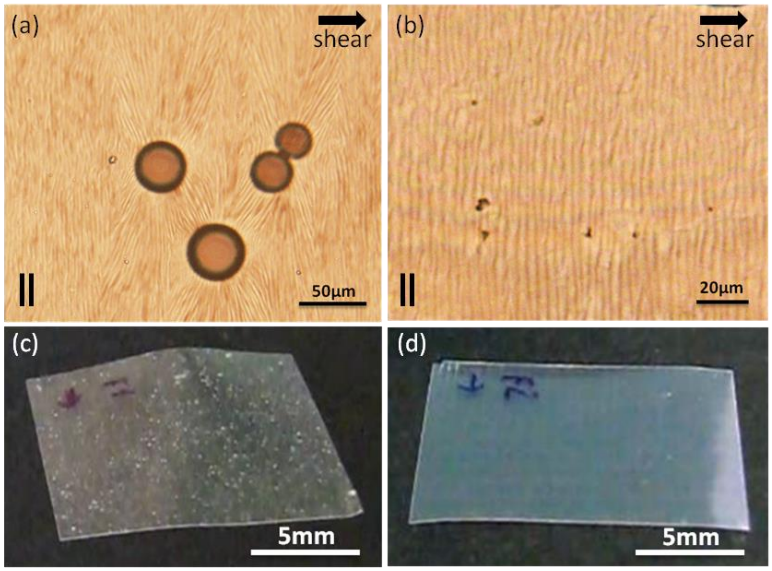

Figure 3.1 – POM images of films of HPC from the supplier (a) Sigma Aldrich and (b) Alfa Aesar prepared from aqueous solutions of 60% (w/w) with parallel polarizers and the corresponding photographs of (c) Sigma Aldrich and (d) Alfa Aesar HPC films. The shear direction is indicated with an arrow. || indicates the polarizers are parallel to each other

Also, it was noticed that for the same speed of casting, HPC from the different suppliers originated films with different thicknesses (ranging from 30μm to 90μm). Specifically, solutions of HPC from Sigma-Aldrich led to films with higher thicknesses. This is consistent with the fact that HPC from this supplier presents a higher viscosity ($\eta = 125cps$) than the one acquired from Alfa-Aesar ($\eta = 89cps$), despite the average molecular weight given by the suppliers being the same.

From the POM images of the surface of anisotropic HPC films, taken between cross-polarizers, a periodicity in the form of gratings was observed along the direction perpendicular to shear, Figures 3.2(a) and (b). After the application of shear, films are left to dry at room temperature. During this process of evaporation the density of mesogenic fragments increases near the top surface given rise to increased orientational order. Since the dimensions of the bottom surface (in contact with the substrate) are fixed and, the increase in order leads to an elongation at the surface in the direction parallel to the shear, the top surface buckles, forming the grooves or gratings, which are locked in the films after the complete evaporation of solvent.[27]

According to the literature, for HPC films, casted from identical lyotropic liquid crystalline solutions, the average distance between grooves is in the order of 3.1±0.3μm [28]. Using the software ImageJ, we measured this parameter for our samples and the values obtained were: 1.8±0.4μm and 3.3±0.7μm for Sigma-Aldrich and Alfa Aesar HPC samples, respectively. As we can see, the measurements for Sigma Aldrich samples are significantly lower than the reference values. Godinho et al. [27] showed that in general the formation of grooves in the HPC anisotropic films is imposed by the shear rate and polymer concentration on the precursor solution. Bearing in mind that the shear rate and concentration of precursor solution are both the same for each HPC used one can only assumed that the average molecular weight of this two HPC sources is not the same. Despite the suppliers presented the same $\overline{M}_w$, two distinct values of viscosity, obtained in the experimental same conditions, are given.

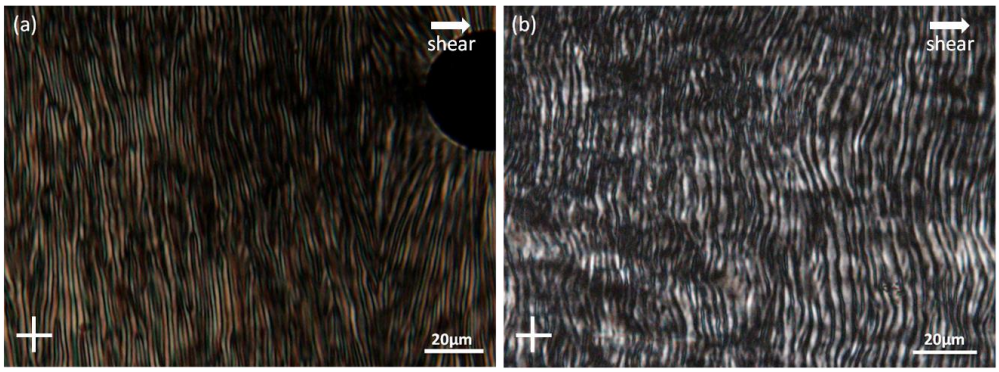

Figure 3.2 - Transmission polarizing optical microscopy images, taken between crossed polarizers of films of HPC from the suppliers (a) Sigma Aldrich and (b) Alfa Aesar, prepared from aqueous solutions of 60% (w/w) and shear-casted with a Gardner knife.

The uniaxial mechanical properties, this is the Young's *moduli*, tensile stress and strain deformation, obtained for films from HPC from both suppliers are presented in Table 3.1. The measurements were taken in the direction (par) of the shear casting and perpendicular (per) to it.

From the observation of this table one can see that values from films of HPC from Alfa-Aesar are in good agreement with the ones found in literature [29], however the same was not observed for the films produced from HPC from Sigma Aldrich. For this later source the values, for most of the parameters studied, are one order of magnitude lower than the values found in literature and obtained in this work by films of HPC from the different supplier.

From table 3.1 it can be seen that all films, prepared from anisotropic solutions, showed a higher Young *modulus* and ultimate tensile strength along the casting direction (Par). The flow induced in these liquid crystalline solutions under the shear stress leads confer a molecular orientation, which results in improved mechanical properties in the direction parallel to the shear.

It is well known the tight relationship between structure and properties in all the materials. According to POM image (in Figures 3.1(a)) and macroscopic appearance (Figure 3.1(c)), samples prepared from Sigma-Aldrich presented some aggregates and major defects. All of this led to films with poor mechanical properties, when compared with the ones prepared from the other source. Recalling the inhomogeneities previously referred, the tensile tests were always performed in different regions of the sample. However, in average, the values obtained for the Young's Modulus and for the ultimate tensile strength were found to be much lower than the ones measured for HPC films produced from Alfa-Aesar.

Table 3.1– Young's modulus (E), tensile stress (UTS) and strain deformation (ε) of the films prepared from an HPC 60% (w/w) water liquid-crystalline solution. *Par* and *Per* means that the mechanical stress-strain measurements were performed along the parallel and the transverse directions to the shear casting direction, respectively

Supplier	E(MPa)		UTS(MPa)		ε (%)	
	Par.	*Per.*	*Par.*	*Per.*	*Par.*	*Per.*
Alfa-Aesar	254±18	154±24	18±2	8±1	39±6	64±22
Sigma-Aldrich	66±5	52±2	9±2	2±1	60±5	*
Previous results [28]	263±39	140±9	17±3	6±2	38±3	60±11

* sample did not fracture

The free surface of HPC solid films was exposed to water vapour and the presence of the vapour leads to a local decrease of the order parameter. Simultaneously is expected that the, during the application of moisture, water molecules will occupy the space between cellulosic chains, which leads to an increase of the thickness of the rod-like fragments. As a consequence, the film's free surface will suffer an expansion in the direction perpendicular to the director. Because of that, when the stimulus is applied, samples will bend around an axis parallel to the shear direction, with the free surface on the outside, as schematic represented in Figure 3.3.

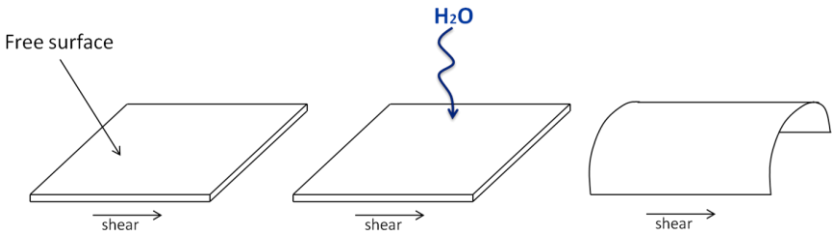

Figure 3.3 - Scheme of a HPC film's free surface (contact with air) bending when exposed to moisture.

Interestingly, the two samples behaved differently when exposed to humidity. While Alfa HPC samples showed a correct dynamics of the bending (according to previous works) [30] as can be seen in Figure 3.4(a), Sigma HPC samples showed an anomalous movement, bending perpendicularly to the shear direction. Also, the response times (6 seconds vs. 26 seconds) were much slower for the latter ones, as it can be seen from images in Figure 3.4(b).

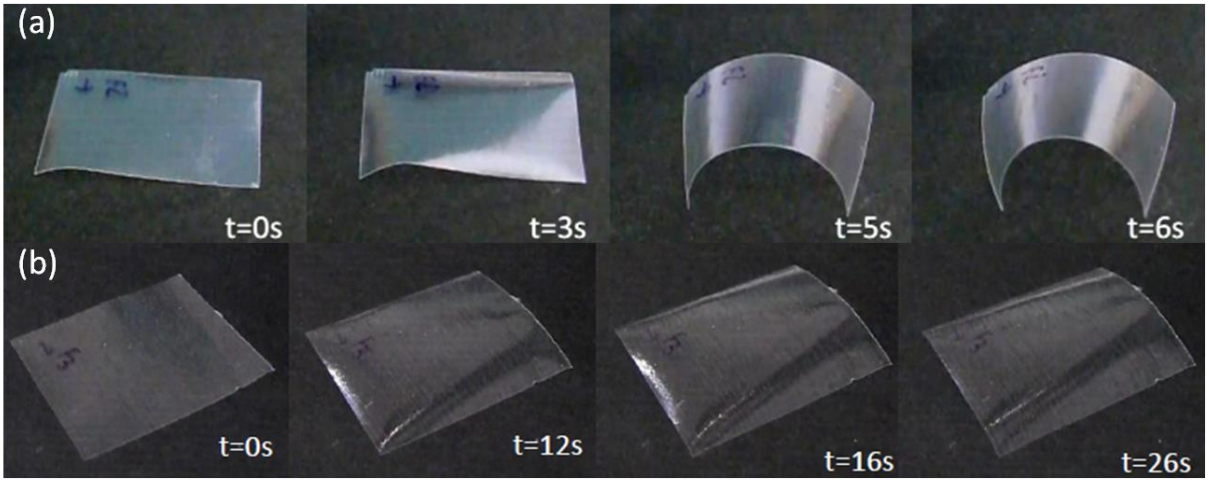

Figure 3.4 – Series of video frames showing the bending of the top surface of free standing films of HPC from the two suppliers (a) Alfa Aesar and (b) Sigma Aldrich, with thicknesses approximately 22 μm and 29 μm, respectively, when exposed to moisture. The shear direction is marked with a blue arrow on the films' surface.

Compared to previous results, where the maximum bending of the free surface of a film with 30 μm was achieved in 8 seconds [30], by decreasing the thickness to 22 μm we were able to accomplish a faster response of about 6 seconds, with the films prepared from HPC solutions of Alfa-Aesar. The unbending time for this sample was approximately 7 seconds, one second lower than the one reported in the literature [30]. Regarding the other sample, the unbending time goes up to 10 seconds.

As the purpose of this work is to optimize the behaviour of the material as an actuator, it was decided to carry on the films' preparation with the HPC solutions from Alfa-Aesar, which had the best properties. Nevertheless, it is important to understand the divergence of behaviours between the two batches of HPC. Despite of having the same average molecular weight, according to the suppliers, the two batches presented a very different viscosity. So one can expect the degree of substitution and/or molar substitution of hydroxypropyl groups per anydroglucose unit of cellulose to be different in each HPC source. In fact, the determination of these two parameters by ^{1}H NMR, showed that the average degree and molar substitution is 1.6 and 4.4 for HPC from Alfa Aesar supplier and 1.8 and 6.0 to HPC from Sigma-Aldrich, respectively, with the substitutional groups attached to different parts of the chain. The detailed determination of the parameters may be consulted in Supplementary Materials – section 6.5. A low DS and high MS can be interpreted as a non-uniform substitution of the cellulosic chain and one can expect that this irregularity would be translated at both micro and nano scale. [31]

3.1.2. Alfa Aesar HPC as Matrix

The x-ray diffractogram obtained for the neat HPC film (from Alfa Aesar) is shown on Figure 3.5. The diffractogram obtained is in good agreement with the one described in the literature for HPC films [32], with the characteristic peaks showing evidence of the HPC major reflections at $2\theta = 8.03°$ and $2\theta = 19.82°$.

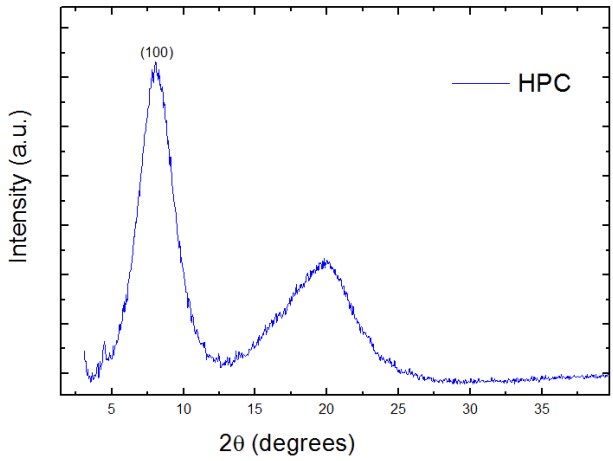

Figure 3.5 - XRD diffractogram for a film of Alfa Aesar's HPC prepared from an aqueous solution of 60% (w/w).

The interplanar spacing was calculated, using Bragg's Law (equation 3.1):

$$\lambda = 2d \sin\theta \tag{3.1}$$

where λ is the wavelength of incident x-rays (λ =1.5406 Å for the experimental setup used), d is the interplanar spacing and θ is the diffraction angle (Bragg Angle). Applying equation 3.1 to the angle corresponding to the (100) plane, the interplanar spacing was calculated to be approximately 1.694 nm.

Based on SEM images (Figure 3.6), a layered structure parallel to the films surface can be observed and also a periodic reminiscent "pins" from a structure, which exists in between the layers. The spacing between the layers observed is of the order of microns.

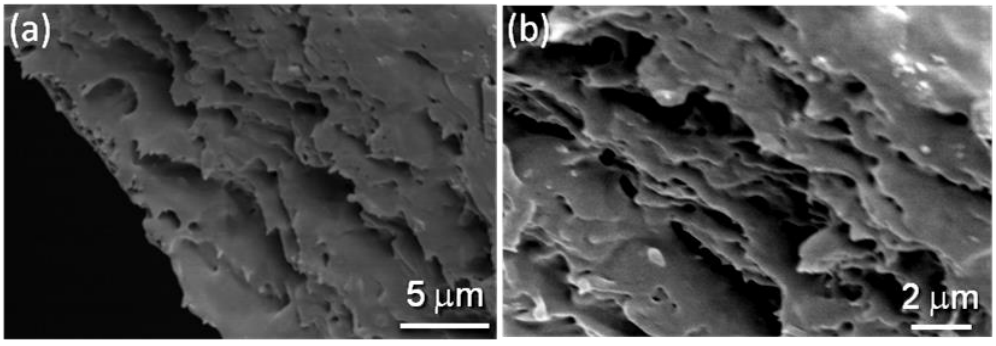

Figure 3.6 - SEM pictures of the cross section of the sheared HPC films. A layered structure parallel to the films surface can be observed with periodic spacing in the range of microns.

In order to understand the influence of the film thickness in the response time, the following was done: films with different thicknesses were produced, using the adaptation developed within this work, which consists in combining different weights on the top of the Gardner casting Knife during the shear casting and also by using two different types of substrates (glass and Parafilm).

For the purpose of the actuators, we only had focus on the films' free surface response (Table 3.2), overlooking the surface that was attached to the substrate – the bottom surface. This option lies in the fact that the bottom surface and the free (top) surface have a slightly different behaviour when the water vapour *stimulus* is applied. Despite the fact that identical bending and unbending response times are obtained [8], the amplitude of the movement is more evident on the top surface than in the bottom. This bottom surface is not so well unravel but one can expected that is less ordered than the top surface, since there is no evaporation of solvent on this bottom surface during shear.

Table 3.2 – Response times for the bending and unbending of free standing HPC films' top surface with different thicknesses

Thickness	**Response time (s)**	
(µm)	*Bending*	*Unbending*
11.3±1.9	7.0±0.3	3.0±0.3
21.1±1.9	7.0±0.3	6.0±0.3
22.2±3.7	6.0±0.3	7.0±0.3

Analyzing the results from Table 3.2, we easily understand that the thinner film has a relatively faster response, especially for unbending. However, thinner films are really difficult to work with, especially during the process of assembly of the device. Also, when the stimulus is applied, these samples tend to saturate much faster, leading to a local dissolution of the sample.

For these reasons, an intermediate thickness was chosen. One must keep in mind that this new chosen film's thickness is lower than the one of the films described in the literature [8], which means, that the response time of our system was improved. Despite the two thicker films having identical thickness, these samples were produced in different substrates, as further described in Supplementary Materials – section 6.2.

3.2. NCC Filler

Nanocrystalline cellulose was chemically obtained via acid hydrolysis of commercial microcrystalline cellulose, as described above. Our intention was to use the NCC as reinforcement in HPC films, to achieve a *stimuli*-responsive material with improved mechanical properties, but mainly improved bending/unbending response times upon stimulus.

It is expected that the properties of the NCCs obtained will have great effect in the overall behaviour of the nanocomposite. For that reason, it is of extreme importance to characterize this promising new composite.

In Figure 3.7 it can be seen the X-Ray diffractogram of a thin film of NCC and its source microcellulose (MCC). This figure shows the same diffraction features for both cellulose materials as the ones observed for semicrystalline cellulose type I (also referred to as native cellulose), which is corroborated by the characteristic peaks at 2θ=14.7°, 16.8° and 22.7° corresponding to the $1\bar{1}0$, 110 and 200 crystallographic planes of cellulose type I, respectively.

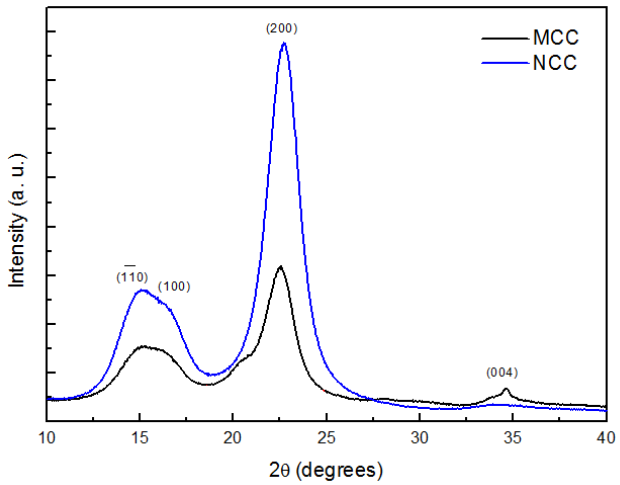

Figure 3.7 – X-Ray diffractograms of the pure MCC source (Avicel) and a thin film obtained from the synthesised NCCs.

The crystallinity index (I_C), which allows comparisons between curves in Figure 3.7, was obtained using the method described in [33]:

$$I_c = \frac{I_{002} - I_{min}}{I_{002}} \times 100 \tag{3.2}$$

where I_{002} and I_{min} represent the crystalline (maximum intensity at a 2θ angle between 21° and 23°) and the amorphous (minimum intensity at 2θ between 18° and 20°) counterparts, respectively.

The crystalline size D_{hkl} was determined using the Scherrer equation [34]:

$$D_{hkl} = \frac{0.9 \times \lambda}{\beta \cos(\theta)} \tag{3.3}$$

where λ represents the X-Ray radiation wavelength, β the Full Width at a Half Maximum (FWHM) of the diffraction peak and θ the Bragg angle.

Solid films prepared from NCC and MCC solutions were also studied. Crystallinity index and crystallite size are summarized in table 3.3. As expected, there was a significant increase in the crystallinity of the NCC film when compared to the source (MCC). This is related to the removal of the amorphous parts of the cellulose. Regarding the crystallite sizes, the NCC film has slightly smaller crystallites when compared to MCC. These results indicate the successful preparation of NCC by acid hydrolysis of microcellulose.

Table 3.3 - Crystallite size and crystallinity index of the NCC film and comparison with the MCC source

	2θ (I_{002})	**I_c (%)**	**D_{hkl} (nm)**
Avicel (MCC)	22.56	76.72	5.39
NCC	22.70	87.82	4.79

FTIR *spectrum* of a NNC film is presented in figure 3.8. One can observe the stretching vibrations of the O-H (3440 cm^{-1}), C-H (2900 cm^{-1}), C-O (1060 cm^{-1}) but also a peak associated with the bending vibration of the O-H at approximately 1640 cm-1 wavenumber, in good agreement with spectra of the nanocrystalline cellulose obtained from similar source.[19]

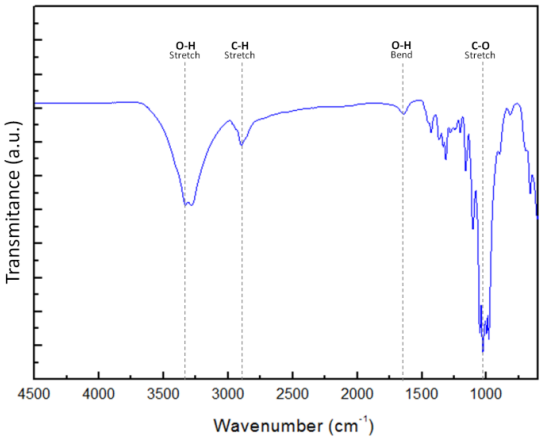

Figure 3.8 - Infrared *spectrum* of a thin film (42 µm) obtained from evaporation of a NCC aqueous suspension (0.6% w/w)

In Figure 3.9, the SEM micrograph shows a dispersion of NCCs prepared from a 0.05% (w/w) NCC aqueous suspension, after drying. Despite the low concentration of NCC used some aggregates are still visible. The average aspect ratio of the cellulose nanocrystals was estimated (from a total of 100 measurements on ImageJ) to be approximately 6.61±2.75 with lengths of 120.80±37.83nm. The length and narrow size distribution are mainly determined by the experimental conditions of the acid hydrolysis, such as time, temperature and pH.

Further details on the statistical distribution are available in Supporting Information, section 6.3.

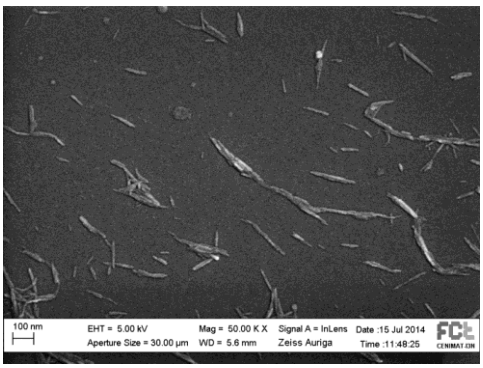

Figure 3.9- SEM micrograph of a dispersion of isolated cellulose nanocrystals, obtained via chemical hydrolysis

Morphologic characterization of a NCC was also obtained by AFM (Figure 3.10). From the top view images of a thin film of NCC it is possible to observed the rod (rice-like) shape of NCCs, as already seen in SEM micrographs. In this case, the microscopy was performed on the surface of a more compact film (instead of isolated NCCs). These images also showed that the rods are very

similar in shape and size in good agreement with the narrow size distribution obtained from SEM images.

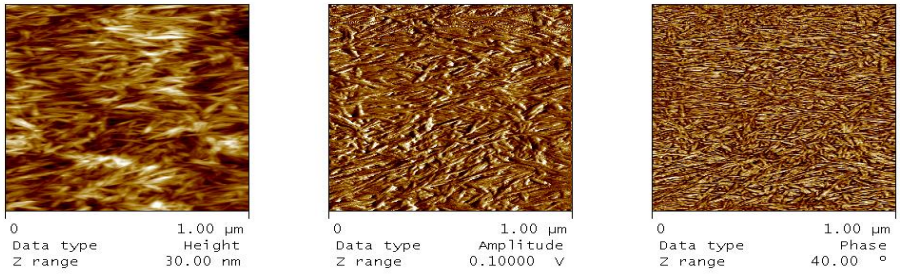

Figure 3.10- Top view images of the surface's amplitude scan of a NCCs' film casted from an aqueous suspension of NCC (0.5% w/w)

3.3. HPC/NCC nanocomposite

The nanocomposites were prepared using HPC and the synthesised nanocrystalline cellulose. The influence of the presence of filler (NCC) on the nanocomposite was studied. In order to maintain the lyotropic liquid crystalline character (and a relatively low viscosity) in the HPC/NCC aqueous solutions, the overall solids content (HPC plus NCC) was kept at approximately 60% (w/w), varying the amount of NCC added. The majority of works described in the literature on HPC/NCC composites [35][13][14][36] were performed at lower concentrations, in the isotropic state. However, in this work we try not only to improve mechanical properties but also to take advantage of the liquid-crystalline properties, for the purpose of the actuator.

Figure 3.11(a) shows the FTIR *spectra* of nanocomposite films with NCC content of 0.05%and 0.83% (w/w). In order to evaluate the influence of the filler in the composite, also a neat film of HPC was analysed. The results (Figure 3.11(a)) show some common peaks for all the samples, i.e. the main stretching vibrations of the O-H (3440 cm^{-1}), C-H (2900 and 2930 cm^{-1}), also peaks associated with bending vibrations can be seen at 1300 cm^{-1} and 1373 cm^{-1} wavenumbers (O-H and C-H, respectively), all of them characteristics from the HPC matrix.[32]

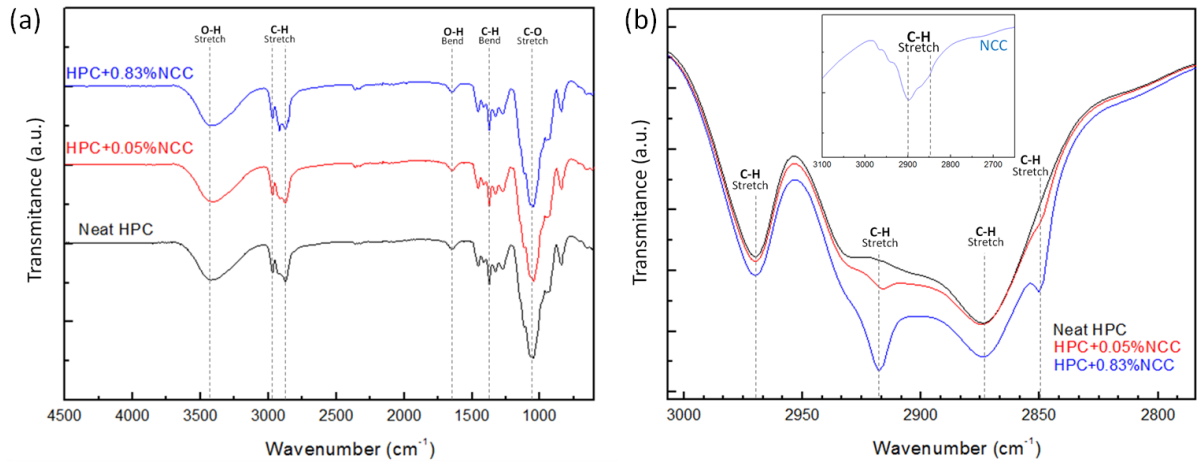

Figure 3.11 - (a) Infrared *spectra* of HPC films with different concentrations of NCC, (b) detailed *spectra* of the same films, where the appearance of a peak at 2918 cm^{-1} wavenumber is observable. The content of solids in the composite is approximately 60% (w/w).

Magnifying the *spectra* for wavenumbers ranging from 3000cm^{-1} to 2800cm^{-1} (Figure 3.11(b)), it is clear the presence of NCC in the composite. The increase of NCC leads to the appearance of peaks at 2918cm^{-1} and 2850cm^{-1}, both corresponding to C-H stretching vibrations of NCC as can be seen in the inset of Figure 3.11 b, that corresponds to the magnification of this region of the spectrum presented in Figure 3.8.

In order to understand the effect of cellulose nanocrystals on the structure of the composite, XRD was performed. When compared to the neat HPC's diffractogram, Figure 3.5, the results obtained for the nanocomposites did not show any obvious variation on the characteristic peaks.

As expected, a higher concentration of nanocrystalline cellulose leads to a higher intensity in the X-Ray analysis, because we are increasing the crystalline fraction of the sample (as shown in Figure 3.12). However, one must keep in mind these are very low concentrations of NCCs.

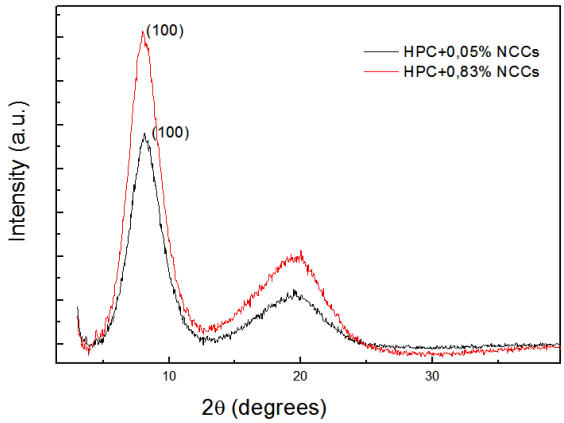

Figure 3.12 – XRD diffractograms obtained for two samples of HPC films with different concentrations of nanocrystalline cellulose incorporated. The content of cellulose in the composite is approximately 60% (w/w).

Identically to what was done for neat HPC, the interplanar spacing was calculated for these composites, also using Bragg's Law (equation 3.1). The obtained values are displayed in Table 3.4. From this analysis, it is quite clear that the interplanar spacing calculated for all the samples presents the same order of magnitude (approximately 1.70 nanometers). Thus, it is not possible to infer conclusively about the influence of the filler in the structure of the composite.

Table 3.4 – Interplanar spacing for HPC samples with different concentrations of nanocellulose

$\%\,\boldsymbol{NCCs}$	$\boldsymbol{2\theta}\ (\mathbf{deg})$	$\boldsymbol{d}\ (\boldsymbol{nm})$
0.00	8.03	1.69
0.05	8.14	1.67
0.83	7.99	1.70

Figure 3.13 shows the three-dimensional topographical image of the free surface of a HPC film with a NCC content of 1.0% (w/w). The image shows a primary set of wider bands, in the direction perpendicular to the shear direction.

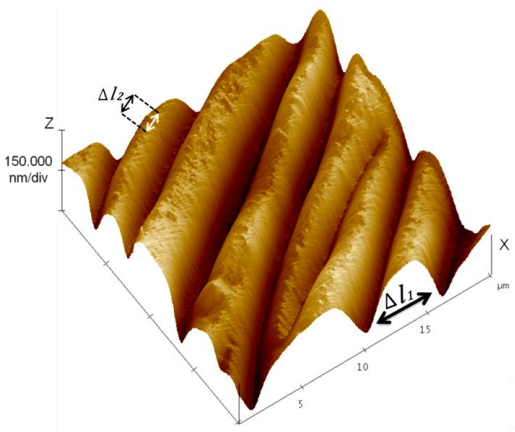

Figure 3.13 – 3D topography image (20×20 μm^2 scan) of the free surface of a sheared HPC film with 1.0% (w/w) of NCC incorporated. The film was prepared from an aqueous anisotropic solution with 60% (w/w) of cellulose and casted at a shear rate of 1.25 mm s^{-1}.

On a closer look, it is noticeable a secondary periodic structure, also in the form of bands, but at a smaller scale and oriented at a small angle to the shear direction. In accordance to previous results, this small angle is approximately 9° [28]. The mechanism behind the formation of the primary set of bands can be attributed to the relaxation of the structure upon drying, after the shear is applied. On Table 3.5 are the average measurements of the periodicity of both sets of bands.

Table 3.5 – Measurements of the periodicities in the surface of a sheared HPC film with 1.0% (w/w) of NCC incorporated, where Δl_1 and Δl_2 represent the spacing between large and small bands, respectively.

$\%\ \boldsymbol{NCC}\ (\boldsymbol{w/w})$	$\boldsymbol{\Delta l_1 (\mu m)}$	$\boldsymbol{\Delta l_2 (\mu m)}$
1.0	2.8-4.4	0.5

The spacing between the primary set of bands for films with different percentages of NCC was also measured based on the POM images presented in Figure 3.14 and the results are shown on Table 3.6. These measurements are in good agreement with the observations from AFM, with values ranging from 3.25 μm to 4.14 μm.

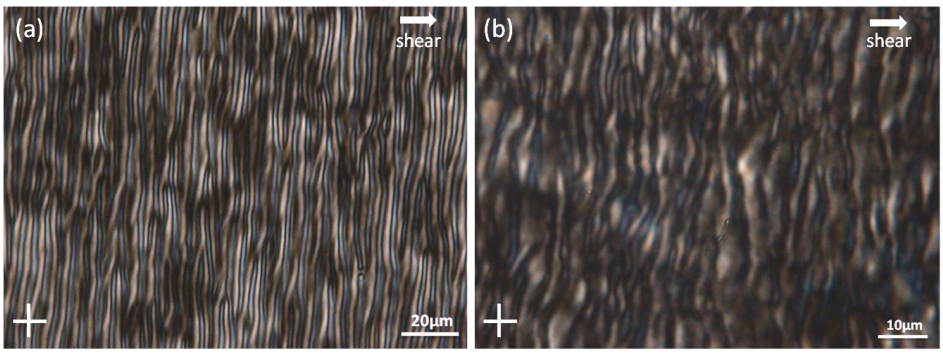

Figure 3.14 - Transmission polarizing optical microscopy images, taken between crossed polarizers of HPC films with (a) 0.40% and (b) 0.83% of NCCs, obtained by shear casting of anisotropic solutions. The shear direction is indicated with an arrow.

It was possible to notice a slight increase of the spacing along with the amount of NCC. A bigger spacing between bands may be an indication that the material is stiffer, due to the incorporation of the

filler. This way, upon drying, the top surface of the film tends not to relax as much as before, leaving wider spaces between the bands.

Table 3.6 – Spacing between gratings in HPC films with different contents of nanocrystalline cellulose. The content of cellulose in the composite is approximately 60% (w/w).

$\%\boldsymbol{NCCs}$	$\boldsymbol{d}$ $(\boldsymbol{\mu m})$
0.00	3.25±0.69
0.40	4.05±0.49
0.83	4.14±0.44

Nanocomposites films of HPC/NNC were characterized by POM, SEM and AFM. In figures 3.15, 3.16 and 3.17, SEM images of the nanocomposites films are presented. The images show that there is a preferential orientation, most likely imposed by the shear. In image 3.15(b) obtained in a cross-section of the film, small grooves are visible, which suggests that the ordering was spread in the whole volume of the thin sample and not only at its top surface. The two kinds of periodicities visible in the AFM image, in Figure 3.15 were also found by SEM, as can be observed in Figure 3.15(b). Simultaneously, Figure 3.15 suggests that the modulation of the small bands is due to the layers' twisting.

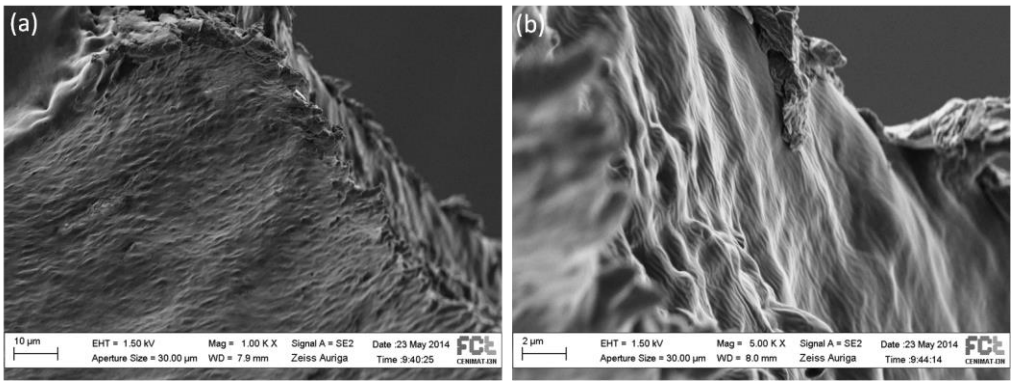

Figure 3.15 –SEM micrographs of a cross-section (perpendicular to the shear casting direction) sample of HPC with 0.05% (w/w) of nanocrystalline cellulose

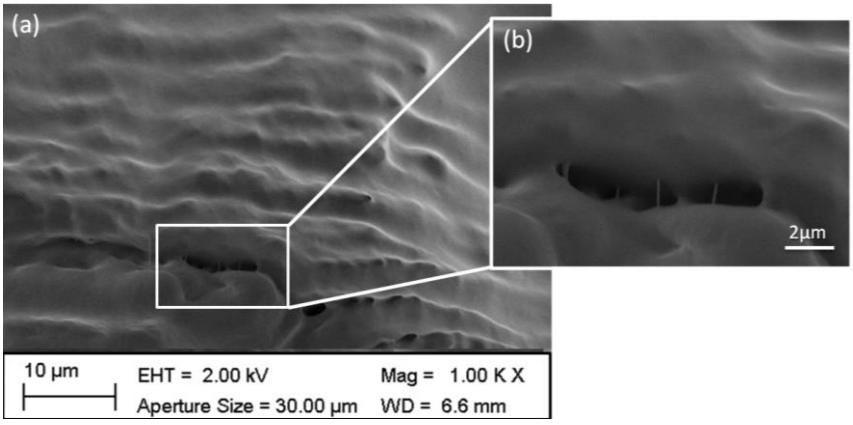

Figure 3.16 - FIB-SEM micrographs of (a) a cross-section (parallel to the shear casting direction) sample of HPC with 2.0% (w/w) of nanocrystalline cellulose and (b) the detail of a fissure between layers.

In figure 3.16, filaments, are observable inside the membrane, between layers, where fissures occur, which are not straight but torsion was noticed, as seen in Figures 3.17(a) and 3.17(b).

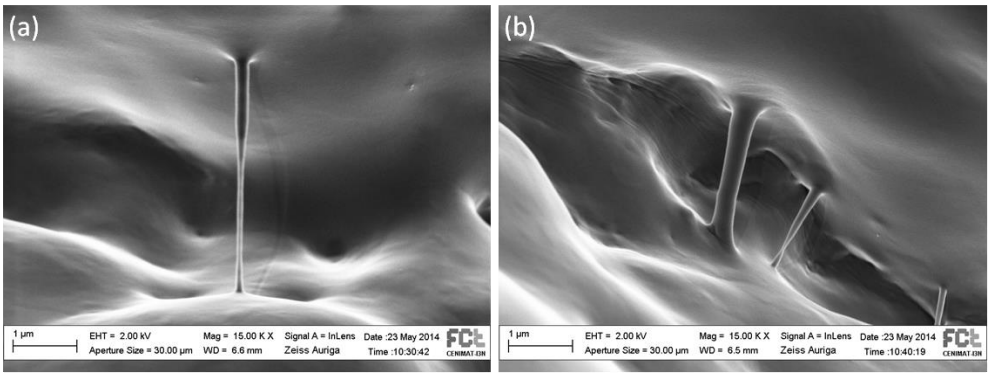

Figure 3.17- FIB-SEM micrographs of a cross-section (perpendicular to the shear casting direction) sample of a film of HPC with 2.0% (w/w) of nanocrystalline cellulose

In Figure 3.18 it is possible to observe the evolution of viscosity with shear rate for HPC aqueous anisotropic solutions with different amounts of NCC.

For these samples, one may observe the typical behaviour of liquid crystalline polymers: for a very small range of low shear rates, it is possible to observe a shear thinning behaviour, followed by the newtonian *plateau* (the molecules are totally oriented inside of domains) with constant viscosity. Increasing the shear rate, the domains tend to disappear, inducing a decrease of the viscosity indicating, again, a shear thinning behaviour.

Apart from the sample with 1 %NCC, for all the other solutions there is a sudden reduction of viscosity for a shear rate of approximately $0.4 s^{-1}$. For the 1%NCC sample, there is an horizontal shift of the flow curve, and consequently, the newtonian *plateau* extends for a wider range of shear rates.

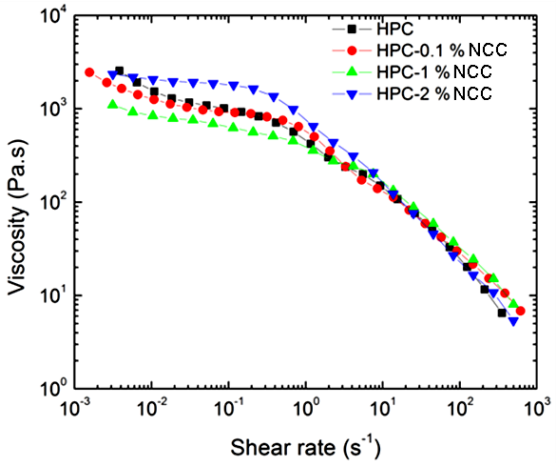

Figure 3.18 - Flow curve experiments for (■) HPC and solutions of HPC with (●) 0.1%, (▲) 1.0% and (▼) 2% of NCCs, obtained at a range of shear rates between 0.001 to 1000 s^{-1}.

In order to determine the viscosity of our solutions and bearing in mind the purpose of studying the overall effects of NCC, one must focus its attention on the newtonian *plateau.* Nevertheless, it is surprising to witness the relation between NCC's concentration and viscosity, which is not

straightforward. Increasing the amount of nanocrystalline cellulose to 1%, there is a decrease of the viscosity, which could be explained by the fact that the NCCs are acting as a plasticizer, favouring the flow. Again, raising the concentration of nanocrystals in solution up to 2%, viscosity tends to increase, as expected.

To study the effect of the presence of NCC in the polymer matrix on the mechanical properties of the HPC/NCC films tensile tests were performed and the results for stress-strain measurements are displayed on Table 3.7. From these, one can see that the physical incorporation of NCC did not induce any appreciable change in the mechanical behaviour of the films. In fact, as seen in table 3.7, the Young's *moduli*, tensile stress and strain deformations obtained for films with the high amount of NCC (0.83%) remain the same as those for the films prepared with pure HPC.

Table 3.7 - Young's modulus (E), tensile stress (UTS) and strain deformation (ε) of the films prepared from aqueous Anisotropic solution of HPC with different concentrations of NCCs. Par and Per means that the mechanical stress-strain measurements

$\boldsymbol{NCCs}$	$\boldsymbol{E(MPa)}$		$\boldsymbol{UTS(MPa)}$		ε (%)	
wt%	*Par.*	*Per.*	*Par.*	*Per.*	*Par.*	*Per.*
0.00	254±18	154±24	18±2	8±1	39±6	64±22
0.05	304±35	201±23	13±2	8±1	44±10	19±4
0.18	224±68	136±32	12±2	5±1	42±8	44±13
0.36	388±64	167±40	20±3	6±1	35±7	80±23
0.83	223±28	211±36	16±2	8±1	43±6	56±18

According to the literature, one could expect that the use of nanocrystalline cellulose as filler in composites would improve its mechanical properties [28]. The lack of improvement in the mechanical properties of the produced films might be related with the low aspect ratio of our filler. It is known that the aspect ratio of the NCCs has a strong influence on this behaviour, and a high aspect ratio give rise to better reinforcing effect in composites. This is mainly due to the need of lower amounts of NCCs to achieve the percolation – this is formation of networks [37][38]. Admitting also that the asymmetry of particles gives rise to a better reinforcement; it would be consistent that our NCCs did not reinforce the material as well as some other results found in the literature.[28]

Some other studies had shown that small amounts of filler were not enough to achieve significant improvements on mechanical properties. A study published by Zimmermann et al. [13], showed that composites of HPC with 1% of reinforcement (NCC) exhibited properties very similar to pure HPC. We should note that in the present study, only concentrations below 1% were tested (for higher contents of NCCs, solutions became highly viscous and, consequently, the films produced were less homogeneous). Overall, the results obtained are in good agreement with those obtained by Zimmermann.

As already been observed in tensile tests of neat HPC films, also these samples showed a higher Young *modulus* and ultimate tensile strength in the casting direction. Once again, this is in good agreement with the molecular orientation induced during the shear casting.

The response observed when water vapour was applied on the top surface of the films, using the same distance between vapour and sample for all the measurements, was observed and recorded. Samples of films, with different percentages of nanocrystalline cellulose, were cut in the shape of squares with dimensions $1.5\text{cm} \times 1.5\text{cm}$.. While during this study, it was noticed that the content of NCCs in the nanocomposite affects the thickness of the films, despite their identical preparation. According to the thickness measurements, displayed in Table 3.8, samples with a lower content of nanocrystals are thinner than the ones with a higher content of NCC, and the increment of 3 times NCC content leads to a film with a double thickness.

Table 3.8 – Thickness for HPC films with identical method of preparation but different content of nanocrystalline cellulose. The content of solids in the precursor solutions was 60% (w/w) in all the samples

$\%\ \boldsymbol{NCCs}$	$\boldsymbol{Thickness}\ (\boldsymbol{\mu m})$
0.5	33.3±2.2
1.0	45.4±5.5
1.5	61.0±4.7

Samples with 0.5% NCCs presented a thickness of 33 μm and a bending time (Figure 3.19(a)) of 6 seconds, similar to the response of thinner neat HPC films (specifically 22μm). Moreover, the unbending (Figure 3.19(b)) was faster than the bending.

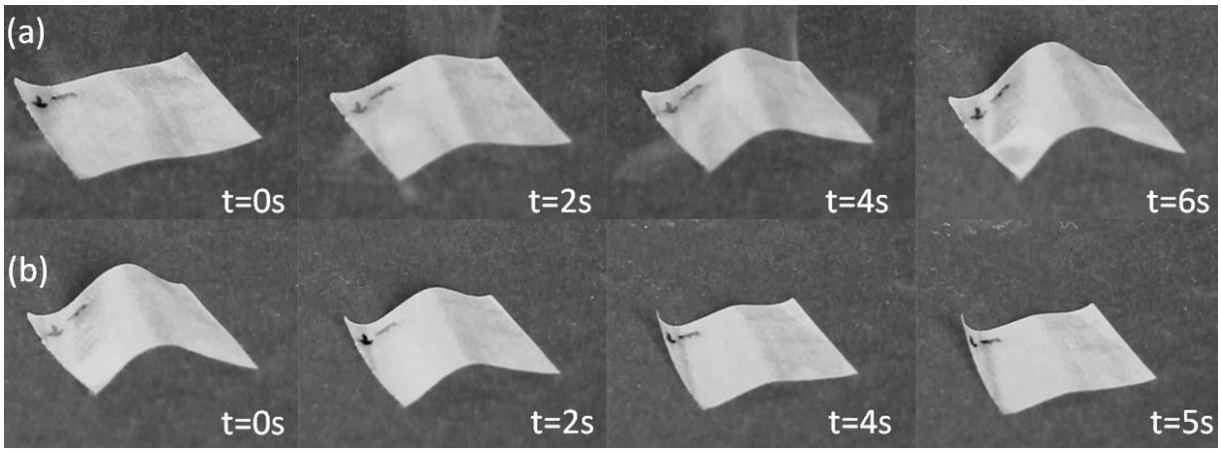

Figure 3.19 – (a) Bending and (b) unbending movement of the top surface of a sample (with dimensions $1.5\text{cm} \times 1.5\text{cm} \times 30\mu\text{m}$) obtained by shear casting of an anisotropic solution of HPC with 0.5% of NCCs. The overall content of cellulose on the aqueous solution was approximately 60% (w/w).The shear direction is marked with an arrow on the films' surface.

A possible explanation can be as follows: NCC, aligned with their main axis along the shear direction, decreases the time to return the equilibrium state, helping the HPC matrix to recover the initial state of order, due to their anisotropic shape (aspect ratio around 7). The response times observed for this sample were better than the ones obtained before, in the literature [8], which represents an improvement of the material's characteristics as an actuator.

For films with 1.0% NCCs were obtained, as referred before, presented a higher thickness when compared to films with lower concentrations. The samples were found to bend around an axis perpendicular to the shear direction, by the action of moisture. A possible explanation for the different behaviour when compared to thinner films can be attributed to the lack of orientation of the entangled polymer molecules along the shear direction and the modulation of the top surface starts to determine the direction of the bending.

Compared with the previous samples (0.5% NCC), these ones take a longer time to bend (Figure 3.20(a)) and unbend (Figure 3.20(b)): 13 seconds and 10 seconds, respectively, by the action of moisture. As noticed before, also for these samples the unbending time is faster than the bending.

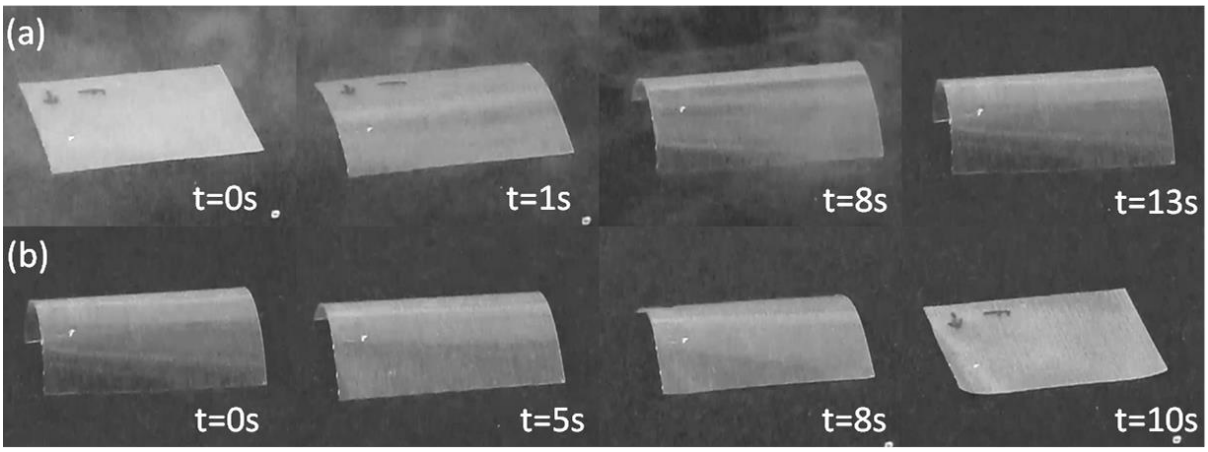

Figure 3.20 - (a) Bending and (b) unbending movement of the top surface of a sample (with dimensions $1.5\text{cm} \times 1.5\text{cm} \times 45\mu\text{m}$) obtained by shear casting of an anisotropic solution of HPC with 1.0% of NCCs. The overall content of cellulose on the aqueous solution was approximately 60% (w/w).The shear direction is marked with an arrow on the films' surface.

One must keep in mind that the moisture affects the order parameter of HPC initially oriented in the matrix in which the NCC rods are immersed. Above a certain content of NCC, the order imposed by HPC molecules cannot determine the behaviour of the system anymore and the films stop to be moisture sensitive. Also by increasing the amount of NCC in the composite (maintaining the percentage of solids), there is less HPC in the films produced. This way, it is easily understandable the slower response times obtained, with the increase of NCC content (and consequently decrease of HPC) in the composite.

As presented in Table 3.8, the thickness measured for the films with a content of 1.5% NCCs is extremely high, around 60μm. As expected, such a thickness does not allow fast response times. In fact, these samples almost did not move and the exposure to moisture was only translated by a slight bending of the surface, as can be seen in Figures 3.21(a) and 3.21(b).

Based in these results, we may conclude that the incorporation of nanocrystalline cellulose as a filler in HPC matrices used as actuators is an option regarding the improvement of response times, especially for the unbending process.

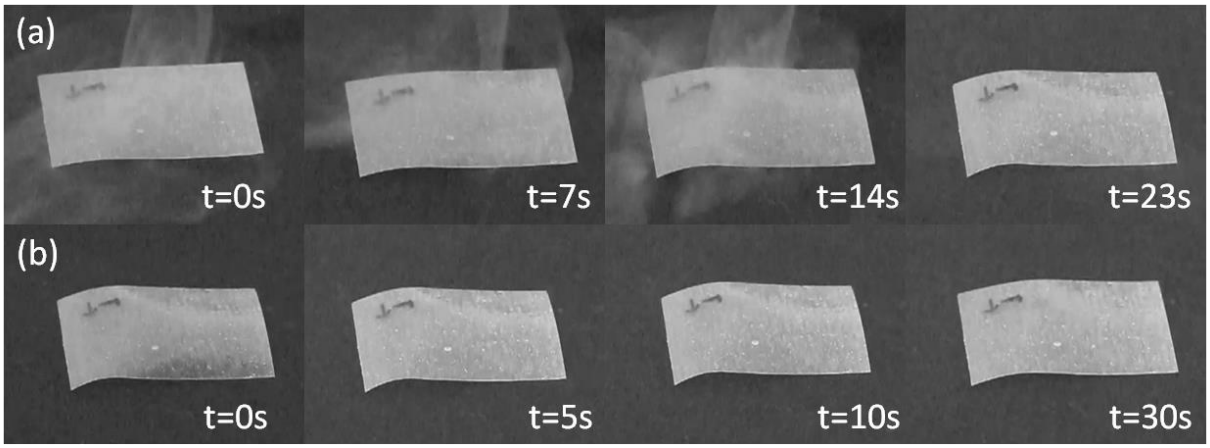

Figure 3.21 - (a) Bending and (b) unbending movement of the top surface of a sample (with dimensions $1.5\text{cm} \times 1.5\text{cm} \times 61\mu\text{m}$) obtained by shear casting of an anisotropic solution of HPC with 1.0% of NCCs. The overall content of cellulose on the aqueous solution was approximately 60% (w/w).The shear direction is marked with an arrow on the films' surface.

Also, the incorporation of this filler leads to a variation in the films' thickness, which means that it could be of interest to produce thinner films with higher percentage of NCCs. Nevertheless, we must take into account some practical limitations. When preparing anisotropic solutions, an excessive amount of NCCs may lead to difficulties during the homogenization step. A non-homogeneous solution, when shear-casted, may originate a heterogeneous film, with aggregates and defects and anomalous response to the *stimulus*.

4. Conclusion and Future Perspectives

In the course of this work, the main objective was to synthesize nanocrystalline cellulose (NCC) to produce stimuli-responsive all-cellulose nanocomposites. In that sense, acid hydrolysis of microcrystalline cellulose (MCC), particle length~50μm, was performed and NCC with average length of 120nm was obtained.. The resulting nanorods were further incorporated in a liquid crystalline aqueous solution of hydroxypropyl cellulose (HPC), with global cellulose content of 60% (w/w).. This way, the incorporation of the nanorods intents not only to improve the response to stimuli of the nanocomposite, but also to take advantage of the liquid-crystalline properties (namely, the self ordering ability) of these systems, for the purpose of creating an improved actuator.

This work was divided in different parts: chemical synthesis of the NCC, preparation of anisotropic solutions, production of *stimuli*-responsive films (by shear casting technique) and study of future applications. The obtained NCC as well as the commercial HPC used and the composite films were characterized via x-ray diffraction, but also by using microscopic and spectroscopic techniques, including SEM, POM, AFM and FTIR. These analyses allowed to conclude that the synthesis was successful and infer about the nanorods' morphology (rice-like shape) and dimensions (aspect ratios 6.61±2.75), as well as crystallinity index and structural information.

NCC obtained presents a higher crystallinity index (I_c=87.82%) than of those of its starting material (I_c=76.72%), due to the removal of amorphous regions of cellulose during the chemical synthesis. Also, the crystallite size determined for the NCC (D_{hkl}=4.79nm) is slightly smaller than the one of MCC (D_{hkl}=5.39nm).

Owing to some problems in the homogeneity in the films initially produced (and consequent poor response to stimuli), HPC from different suppliers (Alfa-Aesar and Sigma Aldrich) were tested. These two systems were well characterized in order to try to establish a relationship between properties and macroscopic behaviour. Based on the macroscopic observation of the films, tensile tests results and primarily from the bending/unbending response times observed after application of water vapour- as a *stimuli*, HPC from Alfa-Aesar presented the best results.

It was verified that thinner films responded faster upon the application of steam. Thin films 'absorb' moisture quicker than thicker ones, leading to a faster response. In order to produce thinner films, the shear casting technique was adapted, being able to drop the minimum speed from 1.25mm s^{-1} to 1.21mm s^{-1}

The influence of the thickness and NCC content in the response time (bending/unbending) of the films was also observed. For films prepared identically, the increase of NCC amount in the composite leads to a direct increase in the films' thickness, as well as an increase in the distance between the macroscopic bands observed at his top surface. This might be due to an increase of stiffness of the lyotropic solution from the presence of NCC, which upon drying cannot achieve the same level of relaxation than those observed for HPC and originate wider space between bands.

Regarding the influence of NCC content in the films, when the concentration is too high (about 1.5%), films tend not to respond. Not only a big amount of NCC is more likely to create aggregates but also, as we maintain the proportion cellulose/water (w/w) in 60%, by increasing the percentage of NCC we decrease the content of HPC. The application of the *stimulus* (steam) induces a response in the HPC matrix. If less HPC is present, the response will tend, gradually, to disappear.

From the rheological results of these composites, no straightforward relation between the content of NCC and the viscosity of solutions could be determined. For a critical concentration, the NCC act as plasticizer, favouring the flow and a decrease in the viscosity. With this essay it was also possible to observe the typical behaviour of liquid crystalline polymers, starting with a shear thinning region, followed by a newtonian *plateau* and an additional shear thinning region for higher shear rates

By adding 0.5% of NCC to films with thickness of 30μm (identical to the previous works), improved response times were achieved. The bending time was shortened from 8 to 6 seconds. Despite the overall improvement, it is of extreme importance to highlight the improvements regarding the unbending time, which was reduced from 8 to 5 seconds. The explanation can be as follows: the anisotropic cellulose nano-rods, in the composite are aligned with their main axis along the shear direction, which helps the HPC matrix to recover the initial state of order. Nevertheless, it was observed that above a critical concentration of NCC, the order imposed by HPC molecules ceases to be the determinant factor of the system and the films stop to be moisture sensitive.

Having in mind the future application of this type of material, a soft steam motor was designed, using a 3D Printer. New features were added, such as the possibility of adjusting the distance between wheels, the use of different wheels' diameters and an exceptional portability. However until now it was not possible to achieve a continuous rotation of the soft motor in this new configuration. Furthermore, for the production of continuous film loops, a mould was designed and manufactured in *Teflon*. By removing the discontinuity in the motor's belt, we will be able to improve its performance.

We acknowledge that there is certainly room for improvement regarding the study of this all-cellulose nanocomposite. For a more complete and deeper comprehension of the *phenomena* involved, some experiments must be performed, such as:

1) Synthesis of NCC with different aspect ratios and further incorporation in cellulosic matrices;
2) Production of films with identical thicknesses but different content of NCC: as the increase of NCC in solution lead to thicker films. By adjustment of the shear-casting equipment, lower velocities could be used for samples with higher amounts of NCC.
3) The use of circular loops for the soft motor.

Regarding the field of applications, this composite has the potential to be employed in a wide range of actuating systems, from electromagnetic generators to artificial muscles. The composite material produced and characterized throughout this thesis showed very promising results, which indicate that in a near future we may be able to produce efficient engines based on soft matter.

5. References

[1] S. Mohanty, “Liquid Crystals - The ’ Fourth ' Phase of Matter,” no. November, 2003.

[2] P. S. Pershan, “Lyotropic liquid crystals,” *Phys. Today*, vol. 35, no. 5, p. 34, 1982.

[3] T. Larsen, A. Bjarklev, D. Hermann, and J. Broeng, “Optical devices based on liquid crystal photonic bandgap fibres.,” *Opt. Express*, vol. 11, no. 20, pp. 2589–96, Oct. 2003.

[4] K. C. Lim, J. D. Margerum, and a. M. Lackner, “Liquid crystal millimeter wave electronic phase shifter,” *Appl. Phys. Lett.*, vol. 62, no. 10, p. 1065, 1993.

[5] M. Collings, J. Hird, *Introduction to Liquid Crystals: Chemistry and Physics*. Taylor & Francis, 1997.

[6] U. Efron, *Spatial Light Modulator Technology: Materials, Devices, and Applications*. CRC Press, 1994.

[7] P. de Gennes and J. Prost, *The Physics of liquid crystals*. 1993.

[8] Y. Geng, P. L. Almeida, S. N. Fernandes, C. Cheng, P. Palffy-Muhoray, and M. H. Godinho, “A cellulose liquid crystal motor: a steam engine of the second kind.,” *Sci. Rep.*, vol. 3, p. 1028, Jan. 2013.

[9] Y. Ji, J. E. Marshall, and E. M. Terentjev, “Nanoparticle-Liquid Crystalline Elastomer Composites,” *Polymers (Basel).*, vol. 4, no. 4, pp. 316–340, Jan. 2012.

[10] J. Shokri and K. Adibkia, “Application of Cellulose and Cellulose Derivatives in Pharmaceutical Industries,” 2013.

[11] R. S. Werbowyj and D. G. Gray, “Ordered Phase Formation in Concentrated Hydroxypropylcellulose Solutions,” pp. 69–73, 1980.

[12] P. Xie and R. Zhang, “Liquid crystal elastomers, networks and gels: advanced smart materials,” *J. Mater. Chem.*, vol. 15, no. 26, p. 2529, 2005.

[13] T. Zimmermann, E. Pöhler, and T. Geiger, “Cellulose Fibrils for Polymer Reinforcement,” *Adv. Eng. Mater.*, vol. 6, no. 9, pp. 754–761, Sep. 2004.

[14] T. Zimmermann, E. Pöhler, and P. Schwaller, “Mechanical and Morphological Properties of Cellulose Fibril Reinforced Nanocomposites,” *Adv. Eng. Mater.*, vol. 7, no. 12, pp. 1156–1161, Dec. 2005.

[15] S.-Y. Lee, D. J. Mohan, I.-A. Kang, G.-H. Doh, S. Lee, and S. O. Han, “Nanocellulose reinforced PVA composite films: Effects of acid treatment and filler loading,” *Fibers Polym.*, vol. 10, no. 1, pp. 77–82, Mar. 2009.

[16] C. Aulin, G. Salazar-Alvarez, and T. Lindström, “High strength, flexible and transparent nanofibrillated cellulose-nanoclay biohybrid films with tunable oxygen and water vapor permeability.,” *Nanoscale*, vol. 4, no. 20, pp. 6622–8, Oct. 2012.

[17] J. Huang, H. Zhu, Y. Chen, C. Preston, K. Rohrbach, J. Cumings, and L. Hu, “Highly transparent and flexible nanopaper transistors.,” *ACS Nano*, vol. 7, no. 3, pp. 2106–13, Mar. 2013.

[18] K. Syverud, H. Kirsebom, S. Hajizadeh, and G. Chinga-Carrasco, “Cross-linking cellulose nanofibrils for potential elastic cryo-structured gels.,” *Nanoscale Res. Lett.*, vol. 6, p. 626, Jan. 2011.

[19] D. Gaspar, S. N. Fernandes, A. G. de Oliveira, J. G. Fernandes, P. Grey, R. V Pontes, L. Pereira, R. Martins, M. H. Godinho, and E. Fortunato, “Nanocrystalline cellulose applied simultaneously as the gate dielectric and the substrate in flexible field effect transistors,” *Nanotechnology*, vol. 25, no. 9, p. 094008, Mar. 2014.

[20] W. F. Smith, *Principles of Materials Science and Engineering*. Hill, McGraw, 1998, pp. 767–829.

[21] T. Eichhorn, S.J.; Dufresne, A.; Aranguren, M.; Marcovich, N.E.; Capadona, J.R., Rowan, S.J.; Weder, C.; Thielemans, W.; Roman, M.; Renneckar, S.; Gindl, W.; Veigel, S.; Keckes, J.; Yano, H.; Abe, K; Nogi, M.; Nakagito, A.N.; Mangalam, A.; Simonsen, J.; Beni, “Review: current international research into cellulose nanofibres and nanocomposites,” vol. 45, no. 1, pp. 1–33, 2010.

[22] M. Yamada, M. Kondo, J. Mamiya, Y. Yu, M. Kinoshita, C. J. Barrett, and T. Ikeda, “Photomobile polymer materials: towards light-driven plastic motors.,” *Angew. Chem. Int. Ed. Engl.*, vol. 47, no. 27, pp. 4986–8, Jan. 2008.

[23] E. D. Cranston and D. G. Gray, “Morphological and optical characterization of polyelectrolyte multilayers incorporating nanocrystalline cellulose.,” *Biomacromolecules*, vol. 7, no. 9, pp. 2522–30, Sep. 2006.

[24] J. F. Revol, H. Bradford, J. Giasson, R. H. Marchessault, and D. G. Gray, “Helicoidal self-ordering of cellulose microfibrils in aqueous suspension.,” *Int. J. Biol. Macromol.*, vol. 14, no. 3, pp. 170–2, Jun. 1992.

[25] W. J. Orts, J. Shey, S. H. Imam, G. M. Glenn, M. E. Guttman, and J.-F. Revol, “Application of Cellulose Microfibrils in Polymer Nanocomposites,” *J. Polym. Environ.*, vol. 13, no. 4, pp. 301–306, Oct. 2005.

[26] N. Triantafillopoulos, *Measurement of Fluid Rheology and Interpretation of Rheograms*. Paper Trade J., 1988.

[27] P. B. M.H. Godinho, J.G. Fonseca, A.C. Ribeiro, L.V. Melo, “Atomic Force Microscopy Study of Hydroxypropylcellulose Films Prepared from Liquid Crystalline Aqueous Solutions,” *Macromolecules*, vol. 35, pp. 5932–5936, 2002.

[28] S. N. Fernandes, Y. Geng, S. Vignolini, B. J. Glover, A. C. Trindade, J. P. Canejo, P. L. Almeida, P. Brogueira, and M. H. Godinho, “Structural Color and Iridescence in Transparent Sheared Cellulosic Films,” *Macromol. Chem. Phys.*, vol. 214, no. 1, pp. 25–32, Jan. 2013.

[29] J. P. Borges and M. H. Godinho, “New bio-composites based on short fibre reinforced hydroxypropylcellulose films,” *Compos. Interfaces*, vol. 8, no. 3,4, pp. 233–241, 2001.

[30] Y. Geng, “Old Cellulose for New Multifunctional Networks,” New University of Lisbon, 2013.

[31] S.N. Fernandes, L. Aguirre, R.V. Pontes, J.P. Canejo, P. Brogueira, E.M. Terentjev, and M.H. Godinho, “Cellulose drivative nanostructures: A fingerprint of Nature,” *Sci. Rep.*

[32] R. J. Samuels and H. Incolpoi, “Solid-state Characterization of the Structure and Deformation Behavior of Water-Soluble Hydroxypropylcellulose *,” vol. 7, no. September 1968, pp. 1197–1258, 1969.

[33] L. Segal, J. J. Creely, A. E. Martin, and C. M. Conrad, “Empirical Method for Estimating the Degree of Crystallinity of Native Cellulose Using the X-Ray Diffractometer,” *Text. Res. J.*, pp. 786–794, 1958.

[34] H. Klug and H. Leroy, *X-Ray Diffraction Procedures: For Polycrystalline and Amorphous Materials*, 2nd Editio. New York: Wiley, 1974.

[35] L. Ma, L. Wang, L. Wu, D. Zhuo, Z. Weng, and R. Ren, “Cellulosic nanocomposite membranes from hydroxypropyl cellulose reinforced by cellulose nanocrystals,” *Cellulose*, Sep. 2014.

[36] T. Zimmermann, N. Bordeanu, and E. Strub, “Properties of nanofibrillated cellulose from different raw materials and its reinforcement potential,” *Carbohydr. Polym.*, vol. 79, no. 4, pp. 1086–1093, Mar. 2010.

[37] Y. Habibi, L. a Lucia, and O. J. Rojas, “Cellulose nanocrystals: chemistry, self-assembly, and applications.,” *Chem. Rev.*, vol. 110, no. 6, pp. 3479–500, Jun. 2010.

[38] B. L. Peng, N. Dhar, H. L. Liu, and K. C. Tam, “Chemistry and applications of nanocrystalline cellulose and its derivatives: A nanotechnology perspective,” *Can. J. Chem. Eng.*, vol. 89, no. 5, pp. 1191–1206, Oct. 2011.

[39] F. F. Ho, R. R. Kohler, G. A. Ward, and H. Incorporated, “Determination of Molar Substitution and Degree of Substitution,” vol. 44, no. 1, pp. 1970–1973, 1972.

6. Supporting Information

6.1. 3D Modelling

The 3D printing process requires a previous modelling of the components, designed in AutoCAD. This resource allows precise dimensions and a total customization of the objects.

Theoretically, and already demonstrated, the motor is able to run using two wheels with the same size. However, it is known that the use of different diameters creates a 'multiplication' effect, providing a better performance. This way, and inspired by the work of Ikeda et. al [22], two wheels were designed with different diameters, as seen in Figure 6.1(a). Keeping the same ratio $\left(\frac{\emptyset_{big\ wheel}}{\emptyset_{small\ wheel}}\right)$=3.33, the wheels were designed with the following dimensions: 3.75 mm for the smaller wheel and 12.50 mm for the larger one, with a height of 5mm for both. Furthermore, a small semi-sphere was carved in the flat surface of the larger wheel, to ease the observation of the wheel's motion when the engine is running. Also a stand was designed, as described in Section 2.3. and shown in Figures 6.1(b) and 6.1(c).

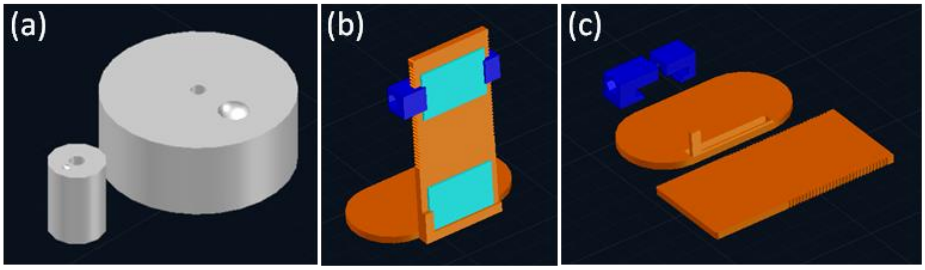

Figure 6.1 – Three dimensional drawings of (a) the wheels and (b),(c) the motor's stand

6.2. Detailed Thickness Study

As described in Section 3.1.2., by combining different substrates and weights over the shear-casting knife, it was possible to obtain films with different thicknesses, as summarized on Table 6.1.

Table 6.1 – Experimental conditions and thicknesses obtained

Substrate	*Parafilm*	Glass	
Weight (g)	191.9±0.1	267.9±0.1	191.9±0.1
Thickness (μm)	21.1±1.9	11.3±1.9	22.2±3.7

Upon the application of moisture, the behaviour of the films was recorded and the response times were measured. The movements of bending and unbending are shown in Figures 6.2, 6.3 and 6.4 for the films with thicknesses $11.3\mu m$, $21.1\mu m$ and $22.2\mu m$.

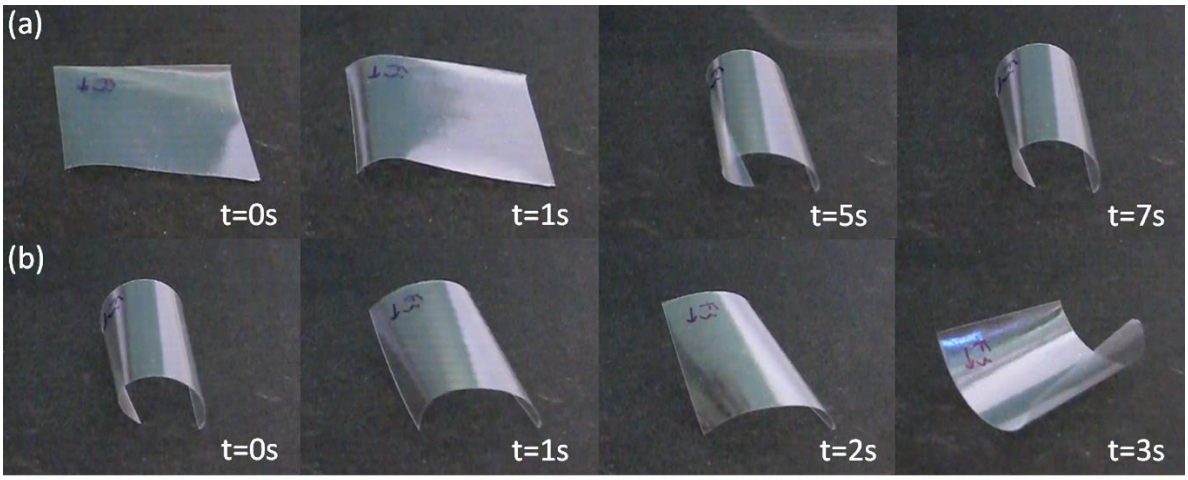

Figure 6.2 – Series of vídeos frames showing (a) bending and (b) unbending movement of the top surface of a sample (with dimensions $\mathbf{1.5cm \times 1.5cm \times 11.3\mu m}$) obtained by shear casting of an anisotropic solution of HPC 60% (w/w).The shear direction is marked with an arrow on the films' surface.

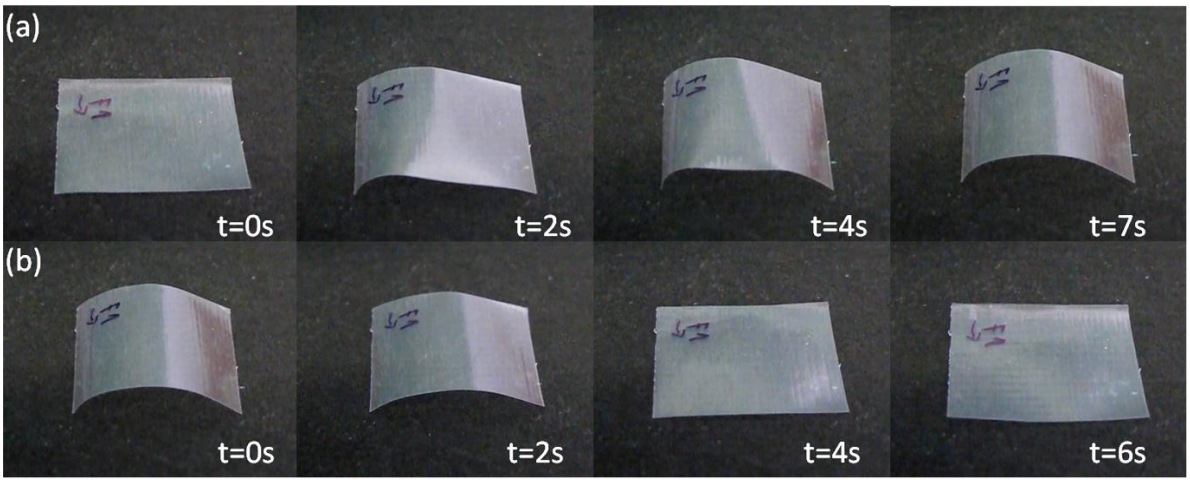

Figure 6.3 – Series of vídeos frames showing (a) bending and (b) unbending movement of the top surface of a sample (with dimensions $1.5\text{cm} \times 1.5\text{cm} \times 21.1\mu\text{m}$) obtained by shear casting of an anisotropic solution of HPC 60% (w/w).The shear direction is marked with an arrow on the films' surface.

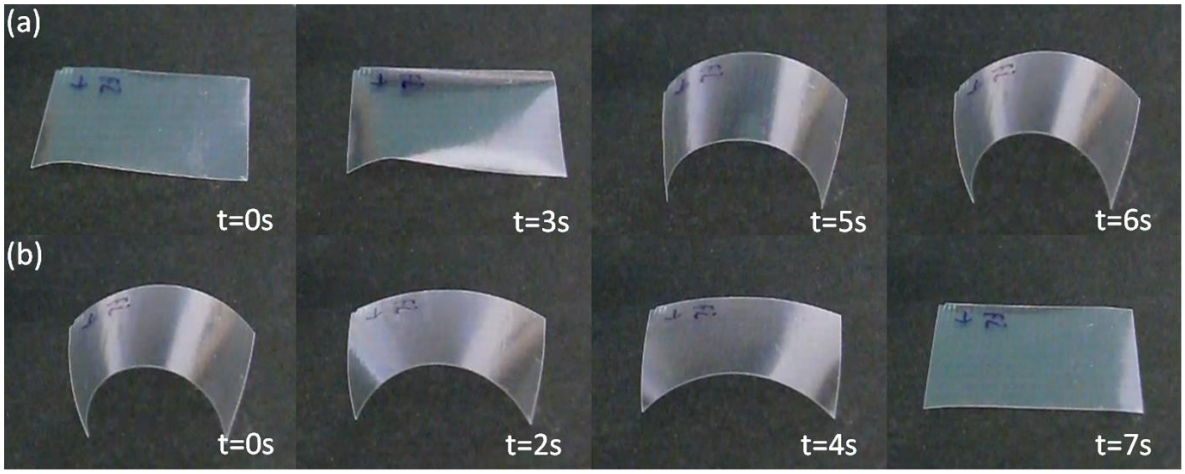

Figure 6.4 – Series of vídeos frames showing (a) bending and (b) unbending movement of the top surface of a sample (with dimensions $\mathbf{1.5cm \times 1.5cm \times 22.2\mu m}$) obtained by shear casting of an anisotropic solution of HPC 60% (w/w).The shear direction is marked with an arrow on the films' surface.

6.3. Statistical Distribution of Aspect Ratios

Based on the SEM micrographs acquired, and using *ImageJ* software, the dimensions of NCC were measured. For this analysis, the images in Figures 6.5 and 6.6 were used.

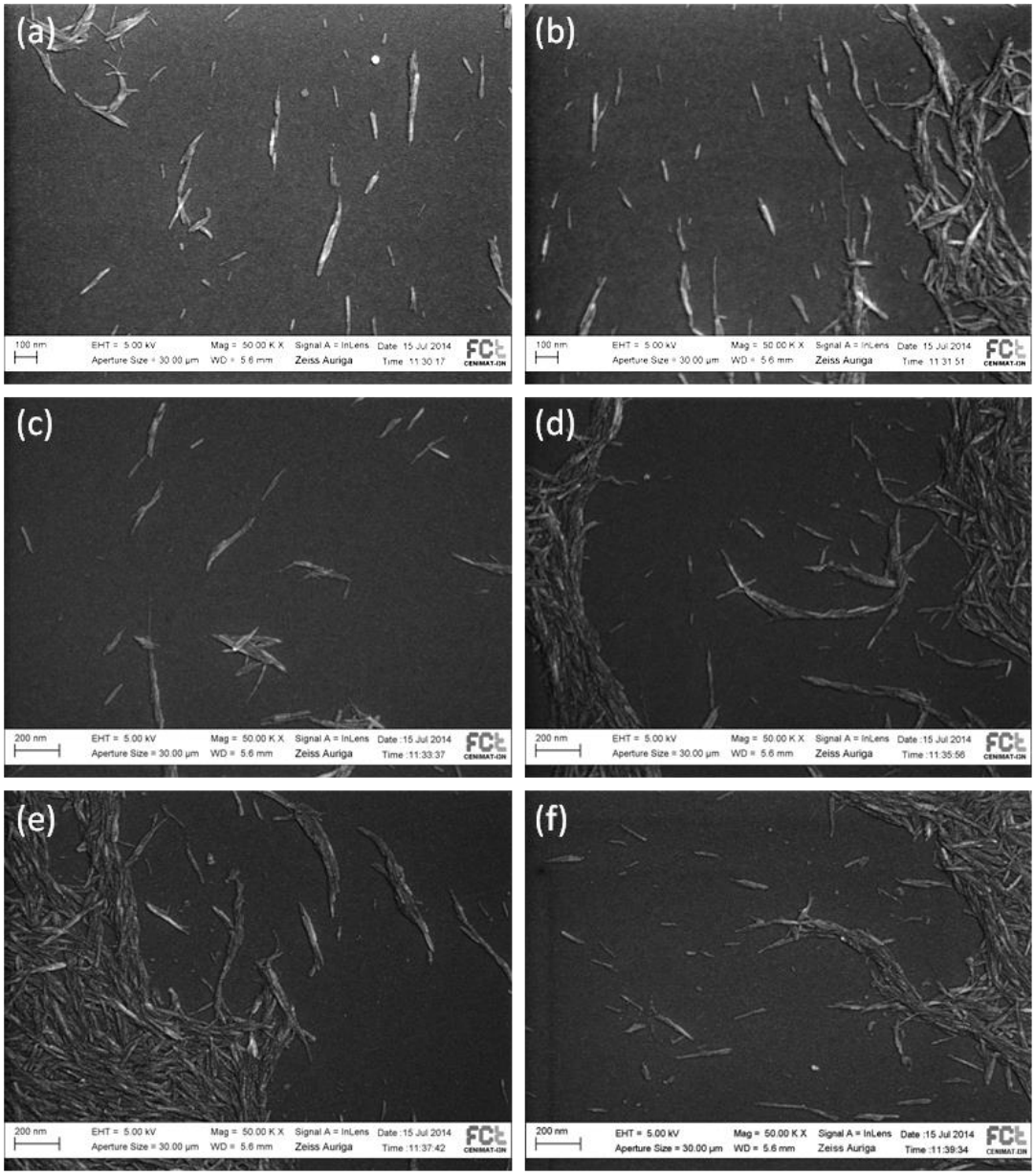

Figure 6.5 - SEM micrograph of a dispersion of isolated cellulose nanocrystals, obtained via chemical hydrolysis

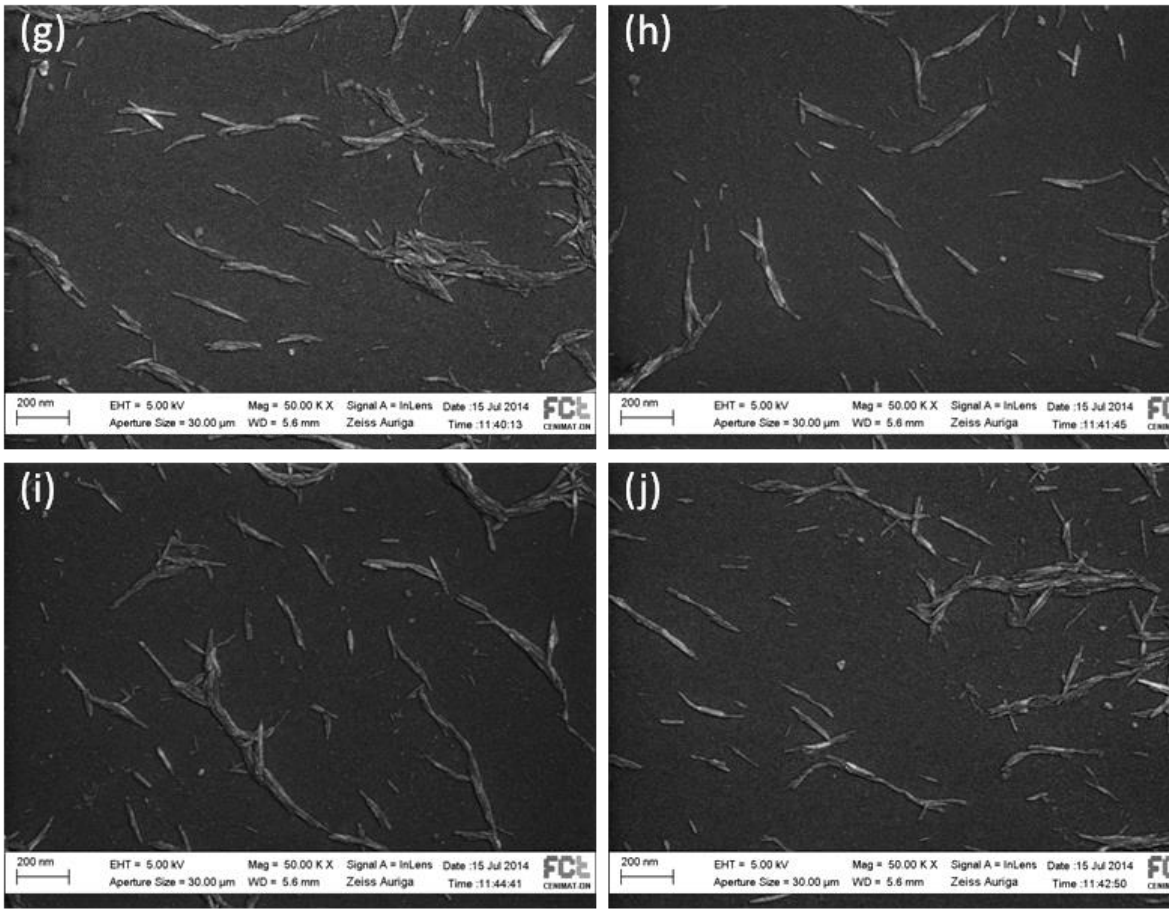

Figure 6.6 - SEM micrograph of a dispersion of isolated cellulose nanocrystals, obtained via chemical hydrolysis.

The measurements taken are displayed in Table 6.2. The correspondence between the images and the measurements is made with the letters from (a) to (j), represented in Table 6.3 and Figures 6.5 and 6.6.

Table 6.2 – Average dimensional measurements and standard deviations

Length (nm)	120±38
Width (nm)	18±5
Aspect Ratio	7±3

Based in the results, it was possible to obtain the Gaussian curve for the aspect ratio, represented in Figure 6.7. The Gaussian function is often used in statistics to describe normal distributions.

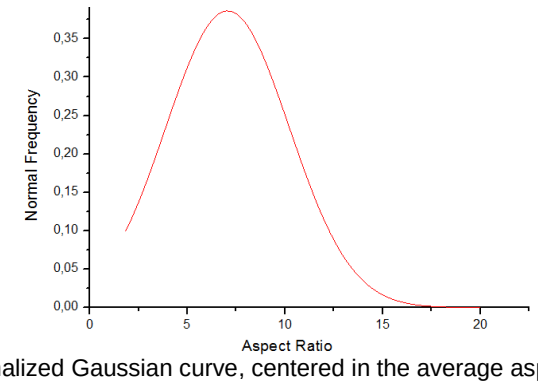

Figure 6.7 – Normalized Gaussian curve, centered in the average aspect ratio calculated

Table 6.3 - Measurements of length and width for SEM images of isolated NCC

		NCCs									
Parameter	**Measurement**	**a**	**b**	**c**	**d**	**e**	**f**	**g**	**h**	**i**	**j**
Length (nm)	**1**	92.486	147.839	140.464	71.841	77.226	106.800	137.667	86.001	114.401	194.953
	2	108.846	80.971	132.278	87.518	103.896	110.962	92.846	159.574	167.184	149.045
	3	95.803	80.971	106.008	40.135	69.937	91.992	107.289	131.280	116.895	115.294
	4	88.415	95.033	169.952	67.305	119.734	74.582	109.536	109.915	81.722	88.932
	5	79.197	70.401	172.903	111.325	88.312	119.504	89.507	171.891	214.010	193.634
	6	87.518	90.312	126.224	170.893	120.828	103.078	147.184	163.443	172.319	137.294
	7	143.246	149.541	131.946	93.335	166.173	134.397	116.703	136.263	81.368	126.043
	8	129.760	98.900	118.050	124.616	130.414	50.559	145.101	101.670	139.677	154.145
	9	-	116.539	167.272	131.846	72.448	120.260	159.815	109.315	124.977	258.153
	10	-	105.149	156.112	114.354	144.827	124.122	73.723	185.732	60.812	187.822
Width (nm)	**1**	18.131	18.977	16.418	20.026	18.981	18.431	20.411	14.762	14.724	16.012
	2	16.418	25.918	21.757	18.490	20.132	18.431	18.256	27.267	11.779	19.280
	3	12.821	13.158	25.253	17.201	15.006	12.909	17.901	21.630	22.427	20.253
	4	15.385	24.826	18.490	13.074	28.864	12.909	20.253	19.773	21.235	17.901
	5	12.821	16.644	27.257	11.467	21.485	21.630	10.127	20.411	15.858	10.741
	6	9.245	16.850	16.217	26.149	21.485	16.983	24.017	17.722	19.754	22.785
	7	27.257	27.974	15.006	12.821	21.485	16.983	12.909	17.901	18.856	17.722
	8	17.949	18.421	24.196	12.821	16.777	20.823	10.438	18.431	35.460	15.190
	9	14.951	19.158	16.777	18.131	15.006	20.823	21.438	14.762	11.779	12.909
	10	10.256	18.977	27.669	10.256	16.777	17.171	17.171	14.762	32.924	10.741

6.4. Production of a mould

To assemble the motor, a stripe of the cellulosic film is cut and bent, in a form of a circular loop, with the free surface on the outside. The two extremities are then joined together (‘glued’) and the loop is placed around the wheels. To optimize the motor’s performance, it could be profitable to eliminate the existent discontinuity in the cellulosic loops, corresponding to the bonding of the two edges. Thus, a mould was designed (seen in Figure 6.8) and produced in Teflon, (to allow removing the films easily from the surface). This mould consists in a central component, where the solution is spread. In an adequate stand, the outer component slides over the inner module, shear-casting the solution, aligning the molecules along the axis of the cylinder.

After drying, the cellulosic loops are cut individually and are ready to be used.

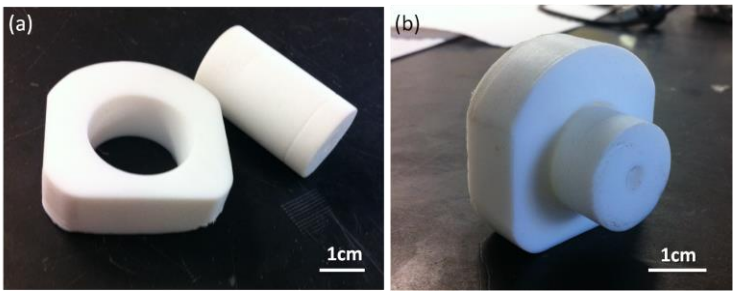

Figure 6.8 – Photographs of the mould produced, with the two components, including an inner cylinder with diameter 2 cm.

6.5. Determination of the average degree of substitution and molar substitution of HPC using ^{1}H NMR

The average degree of substitution of HPC is defined as the number of the substituent hydroxypropyl groups per Anydroglucose (AGU) units of cellulose, and the maximum value for $\overline{DS}$ is 3, since only 3 -OH groups are available in each AGU unit. The new hydroxypropyl group added on the cellulose chain also has a hydroxyl group that can also undergo further substitution, by adding another hydroxypropyl group, this process can be repeated indefinitely and this number is defined as molar substitution. In figure 6.9, it can be seen one of many possible structures of HPC with a molar and degree of substitution of 4 and 2.5, respectively. These numbers can be determined by NMR spectroscopy.

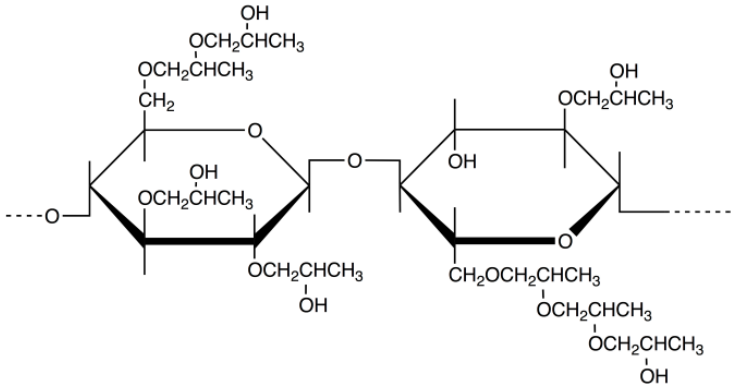

Figure 6.9 - Scheme of a possible molecular structure of hydroxypropylcellulose with a molecular substitution of 4 and a degree of substitution of 2.5.

^{1}H NMR spectra of HPC, from both suppliers, in $CDCl_3$ (used as internal reference) were recorded with a Bruker ARX 400 spectrometer at 400 Hz. From the ^{1}H NMR spectrum of HPC the following equations (6.1) and (6.2), based on the work of Ho et al. [39] , were used to calculate the $\overline{DS}$ and $\overline{MS}$:

$$\overline{DS}_{HPC} = \frac{10I_{CH_3}}{3I_g + I_{CH_3}} \quad (6.1)$$

$$\overline{MS}_{HPC} = \frac{10I_{CH_3}}{3(I_g - I_{CH_3})} \quad (6.2)$$

where I_{CH_3} correspond to the integrated areas of the methylene groups, that appear around 1.0 ppm and I_g is the integrated area of the corresponding protons of AGU of cellulose (7 CH and 3 OH), that appear in the chemical shifts 4-3 ppm.